Sustainable Energy & Fuels

REVIEW

View Article Online
View Journal | View Issue

Cite this: *Sustainable Energy Fuels*, 2022, **6**, 243

Progress and challenges on scaling up of perovskite solar cell technology

Jin Yan, [a] Tom J. Savenije, [b] Luana Mazzarella[a] and Olindo Isabella *[a]

Since the first application of a metal halide perovskite (PVK) absorber in a solar cell, these materials have drawn a great deal of attention in the photovoltaic (PV) community, showing exceptional rapid progress in power conversion efficiency. The potential advantages of low-cost, high efficiency, easy processability, and wide range of applications make PVK solar cells (PSCs) a desirable candidate for future uptake in the PV market over traditional semiconductors such as silicon. Furthermore, PVK thin-film technology holds a concrete potential to closely approach the theoretical efficiency limit for single-junction solar cells *via* unique control of the optoelectronic properties. However, for a disruptive breakthrough of PVK technology from fundamental research to industry, systematic research efforts are required to unravel the poor long-term stability and to reach a reliable large area fabrication process. In this review, we examine in detail recent progress on large-scale PSCs and we discuss challenges for commercialization touching upon the following aspects: material properties, fabrication technology, and industrialization challenges. Besides, the long-term stability and efficiency of large-area PSCs as well as PVK-based two-terminal tandem devices are discussed. In addition, strategies for PSC upscaling are further studied for scalable deposition technologies. Finally, we review the most recent literature on costs and environmental assessment.

Received 7th July 2021
Accepted 24th November 2021

DOI: 10.1039/d1se01045j

rsc.li/sustainable-energy

1. Introduction

Photovoltaic (PV) technology converts solar energy into electricity. Over the last seventy years, many different absorber materials and device architectures have been developed resulting in high power conversion efficiencies (PCEs). Among them, crystalline silicon (c-Si) and so-called III–V solar cells have demonstrated high efficiencies and a mature level of development. Currently, c-Si solar cells dominate more than 90% of the PV market share[1] because of cheap raw materials, long stability, and well-established technology. However, the limitation of c-Si PV is the complex fabrication process as well as high requirements for wafer quality, which increase the fabrication cost and hinder further commercialization of high-efficiency architectures.[2–4] The promise of emerging thin-film PV technology is to cost-effectively fabricate high-quality semiconductor materials by simpler deposition processes and reducing the amount of material used.

Over the last decade, organic–inorganic metal halide perovskite (PVK) has attracted much attention in the PV research community, after Kojima *et al.*[5] discovered in 2009 the ability of PVK to convert the energy carried by sunlight into electricity. The reasons behind the success of PVK can be ascribed to its exceptional electrical properties with direct bandgap and high absorption coefficient, long carrier diffusion length, tuneable bandgap by compositional engineering, and simplified deposition process. With these outstanding properties, PVK solar cells (PSCs) have been developed rapidly, demonstrating in only a decade, albeit on a sensibly smaller device area, PCEs approaching those recorded by solar cells based on c-Si.[6]

However, compared to c-Si, PVK technology still has two main drawbacks namely device stability and device upscaling. These two factors directly determine the steps toward commercialization. Pinholes and defects existing in thin films have a negative impact on photoelectric properties[7,8] and their influence becomes more severe for an effective lab-to-fab transition.[9] To address this problem, various scalable deposition strategies are employed for each layer of the PSC to obtain high-quality films and excellent device properties. Challenges in device stability, as well as cost including environmental impact, are all crucial topics of relevance for the PV industry.

In fact, PVKs suffer from different degradation pathways related to temperature,[10,11] humidity,[12,13] composition,[14] and light.[15,16] This leads to decomposition of the material and decrease of performance as time goes on. Several approaches[17–20] have been explored to prevent this reduction in performance. Recently, PVK degradation mechanisms have been reported[21] and different materials are tested to replace less stable systems.[22] Up to now, large-scale (100 cm^2) PSCs show

[a]*Photovoltaic Materials and Devices, Delft University of Technology, Mekelweg 4, 2628 CD Delft, The Netherlands. E-mail: O.Isabella@tudelft.nl*

[b]*Department of Chemical Engineering, Delft University of Technology, van der Maasweg 9, 2629 HZ Delft, The Netherlands*

promising stabilities.[23,24] Nevertheless, there is still a long way towards commercialization, especially compared with c-Si PV. An approach to control degradation deals with tailoring the nature of the PVK lattice by using various cations[25] and halide anions.[26,27] Other strategies comprise functionalizing the PVK material to improve stability.[28]

Although there are numerous challenges, the progress of PSCs towards commercialization is unprecedented in the PV community. Many technologies are demonstrated to be suitable for scalable film deposition, which can produce each layer of PSC with high film quality. With the application of various strategies, such as precursor engineering and interfacial engineering, the efficiency for large area devices has been largely improved. PSCs with an active area of more than 57 cm^2 have been fabricated with a certified PCE of 14.6%.[29]

Besides, PVK is also employed as at least one of the absorbers in double and triple-junction solar cells fully based on PVK PV technology[30–32] or in combination with c-Si PV technology. For their promising PCEs, the PVK-based tandem solar cells provide a valuable economic approach to break through the Shockley and Queisser (SQ) limit[33] for single-junction devices. Currently, the world record PCE for PVK/c-Si tandem solar cell has achieved 29.8%.[34] Apart from efficiency, long-term stability has also been improved in the last years with the introduction of inorganic cations, such as cesium (Cs). Nowadays, large-area devices are reported to work consistently for 1000 h under the condition of 25 °C and 85% humidity with an area of 25 cm^2.[35] With further development of encapsulation technology and device optimization, the device stability aims at fulfilling the test requirements for commercialization in near future.

In this review, we discuss recent progress in large-scale PSCs and focus on the challenges for commercialization. Section 2 summarizes several high-volume manufacturing technologies which are suitable for scalable deposition of PVK film. Section 3 summarizes the challenges of up-scaling for different PVK layers. Section 4 provides an overview of efficiency and stability for large area PVK-based monolithic tandem solar cells. Additionally, to have a reasonable assessment of PVK industrialization, cost and environmental impact are discussed in Section 5. Finally, we review several companies which have started their business using PSCs for a variety of applications.

2. Progress for scalable techniques

Fabrication of uniform and pinhole-free large-area PVK films can be realized by employing suitable deposition methods, such as blading, slot die coating, spray deposition and more. In this section, we review some deposition methods enabling scalable processes for PVK film fabrication.

2.1 Solution based processes

2.1.1 Blade coating. In the blade coating process, the precursor solution is spread onto a substrate by a moving blade, forming a wet film, as shown in Fig. 1a.[29] The film quality depends on the properties of the substrate surface,[36] velocity of the blade, solvent properties (for example composition,[37] concentration, solvent viscosity),[38,39] annealing temperature,[40] and atmosphere. As an example, Fig. 1b illustrates the relationship between coating speed, film thickness, and solvent evaporation.[29] Since the first PVK film was formed with blade coating in 2015, many studies have been reported ranging from *in situ* observations to technical optimization.[41,42] *In situ* grazing-incidence XRD measurements are employed for blade coating to observe the ink-to-solid phase transformation of PVK films during preparation.[43] The composition, solvate phase, and intermediate complexes are observed under low processing temperatures; the crystallization process takes place directly without forming intermediate phases, leading to a successful method for large-area film fabrication.[43] Apart from the *in situ* observation of PVK crystallization, various basic technical parameters are also optimized. Temperature and solvent evaporation rate are of critical importance to control the film formation.[44] Kim *et al.*[45] found that a slow solvent drying process could encourage the formation of large crystals, which were formed immediately after solution blading. In Mallajosyula's work,[40] a temperature-controlled blading technique was employed for the growth of large-grain PVK thin films. Apart from temperature, other parameters, like coating speed, is found to have a relationship with film thickness, which is clearly explained in Horizontal dip-coating regime.[46] Besides, a combination of blade coating and rapid thermal processing has been demonstrated to exhibit high PVK film quality.[40] Devices with a PCE over 17% for an active area of 2.7 cm^2 were reported.[47] The interaction between the ink and the substrate was also investigated. Dai *et al.*[36] introduced ammonium chloride as an additive into precursor solution to reduce film trap density, flexible PSCs with a record PCE of 15.86% was obtained for an aperture area of 42.9 cm^2 (see Fig. 1c). Similarly, Chen *et al.*[48] recently partially replaced dimethyl sulfoxide with solid-state carbohydrazide to avoid the formation of voids at perovskite–substrate interfaces. Based on the research mentioned above, this technique shows a high sensitivity towards temperature and towards the interaction between the ink and the substrate. Blade coating approach is flexible to combine with other methods to prepare PVK films, such as roll-to-roll setups, rapid thermal processing,[40] and sequential deposition,[38] which provides more possibility for the future commercial application.

2.1.2 Spray coating. The spray coating technology was firstly used for PVK preparation in 2014 (ref. 51) and developed rapidly from then on with various ways of creating the spray droplets. In this process, tiny liquid droplets are formed with a nozzle and then dispersed onto a substrate, as shown in Fig. 1d and e. According to the investigation of Chen *et al.*,[52] the spray process is classified into three stages: (i) atomization process, (ii) droplet flight, and (iii) film deposition. Each of them was discussed in detail from principles to parameters in ref. 52. The flying route of these tiny droplets during spray has a strong influence on the final film quality. Ishihara *et al.*[53] studied the fluid dynamics of droplets and Girotto *et al.*[49] described the relationship between spray velocity and precursor solution spreading capabilities. Besides, factors affecting the deposition were systematically optimized, such as precursor

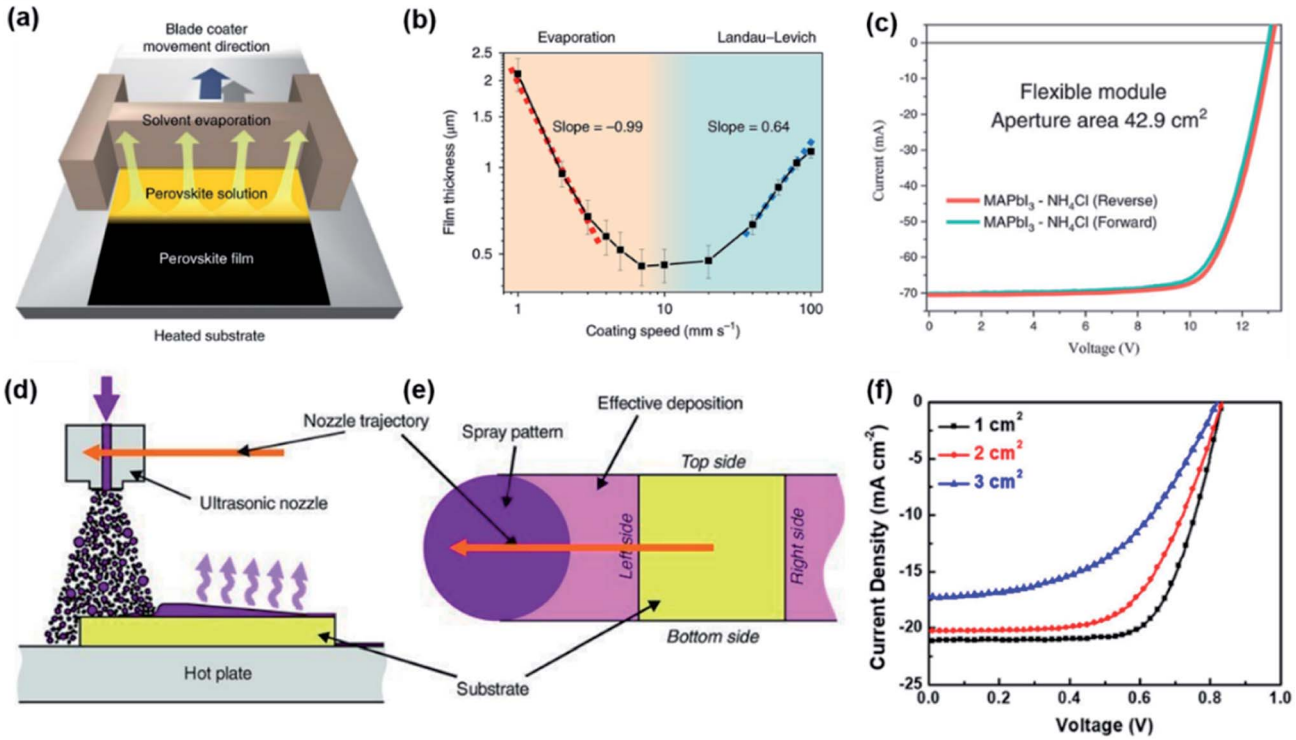

Fig. 1 (a) Diagram of blade coating of PVK film[29] (b) the film thickness as a function of coating speed for blade coating[29] (c) *J–V* curves for flexible PSCs with a record aperture area of 42.9 cm^2 and PCE of 15.86% (ref. 36) (d) diagram of the spray coating process[49] (e) diagram of the magnified structure of nozzle trajectory[49] (f) *J–V* curves for PSCs with different active areas.[50]

solution (viscosity, concentration, compositions),[54,55] substrate (wettability, roughness, temperature),[56,57] boiling point of solution,[58] distance between the nozzle and substrate.[59] Park *et al.*[56] prepared high-quality PVK layers by controlling the flow rate of precursor solution and the reaction temperature. As a result, larger-scale PVK film with an area of 7.5 × 7.5 cm^2 showed excellent photovoltaic properties and uniformity.[56] Chou *et al.*[50] realized a PCE of 7.01% with an aperture area up to 3 cm^2 by controlling precursor solution concentration and spray passes; the corresponding *J–V* curves are shown in Fig. 1f. Recently, Heo *et al.*[60] successfully prepared $CsPbI_{3-x}Br_x$ sub-module by spray coating with an efficiency of 13.82% (112 cm^2 aperture area). A graded PVK absorber structure is created and it shows only 9% degradation after 1-sun light soaking for 1000 h.[60] All-spray coating PSCs (CTLs and PVK) have also been reported,[61] and PCEs are in the range of 10–12% with an aperture area of about 1 cm^2. Spray coating of PVK PV shows an increasing PCE situation in the recent few years and the future experiments can concern more about low volatility controlling, new additives for PVK solution and novel transport materials.[59]

2.1.3 Slot-die coating. Slot-die coating can be applied for film deposition of different layers, especially the PVK layer. During the process, the coating head is positioned close to substrate and there is a narrow slit on the coating head. Precursor solution is pumped into the coating head and is forced to flow out of the narrow slit onto the moving substrate. The film quality is extremely sensitive to the processing parameters such as the substrate temperature, wettability, moving speed, and width of the slit. Besides, the wettability, viscosity of precursor solution also influences the degree of PVK crystallinity.[62,63] In Cotella's work,[64] the preheated substrate combining with air-knife led to a temperature gradient in the wet film which plays a crucial role in controlling the crystallization. By selecting low boiling solvents and employing multifunctional additives, the processing window time can be widened. The Dutch institute Solliance, which is specialized in the roll-to-roll slot die production process of PVK layers,[65] has modified the ink with a co-solvent and additive, avoiding efficiency losses with the increase of area during the drying process. They demonstrated a 144 cm^2 module with a PCE of 14.5%.[66] Apart from the physical property influence of precursor solution, chemical properties such as additive[67,68] and composition[69,70] can also lead to excellent film properties. By applying additive method, Yang *et al.*[71] prepared large-area FACs based perovskite films with a certified quasi-stabilized efficiency of 16.63% (20.77 cm^2). Besides several basic parameters, models and principles are also introduced to further explain the slot die coating process. Xu *et al.*[72] investigated the infiltration process of the precursor solution into a mesoporous titanium oxide (TiO_2) according to the Lucas–Washburn model.[73] Under the guidance of the model, coating parameters were optimized and a PCE of 12.87% was obtained with an active area of 60.08 cm^2.[72] Fig. 2a and b show the device structure and corresponding *J–V* curves.[72] Bu *et al.* prepared 65 cm^2 FACs-based PSCs with a certificated PCE of 19.54%. In their work, avoiding the formation of PVK intermediate complex is the key point to

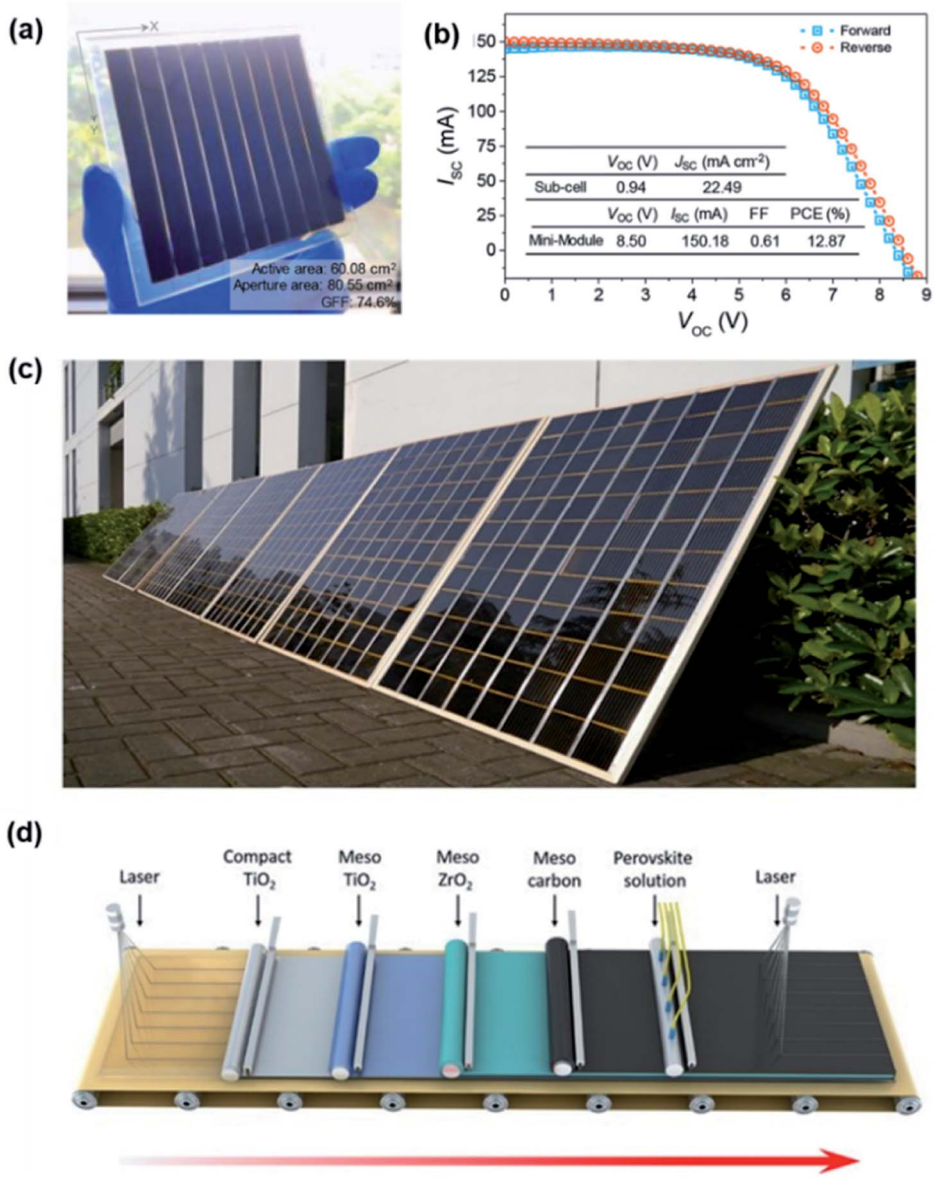

Fig. 2 (a) Image of slot die coated PSC-based mini-module with an active area of 60.08 cm^2;[72] (b) the *J*–*V* curves of the device shown in (a);[72] (c) image of 7 m^2 fully printed PSC-based modules;[80] (d) diagram of fabrication process for fully printed PSCs.[80]

obtain high quality PVK film.[74] Not only for PVK film formation, but deposition of CTLs can be also realized with slot-die coating. All-slot-die coating devices with PCEs around 11% have been successfully fabricated.[75–77] Among all-slot-die coating works, Di Giacomo *et al.*[78] in Solliance fabricated PVK solar modules; the highest PCE exceeded 10% with a power output of 1.7 W for an area of 168.75 cm^2. Slot-die coating shows a great potential toward industrialization because it is one of the most used techniques for the roll-to-roll fabrication of PSCs.[79]

2.1.4 Inkjet printing. In terms of inkjet printing, precursor solution is dispersed by nozzles. The influence of some basic factors (such as substrate wettability, temperature, ink droplet wetting behavior, viscosity, and solvent evaporation rate) on PVK film quality was investigated. Properties of the precursor solution play an important role in controlling PVK film formation.[81] Li *et al.*[82] reported a new ink system, whose solvent was composed of *n*-methyl pyrrolidone (NMP) and dimethylformamide (DMF), because NMP can effectively adjust the viscosity and surface energy of the precursor solution. As a consequence, devices were fabricated with PCEs of 14.5% (4.04 cm^2).[82] As the most basic factor, temperature is also taken into consideration. In Liang's work,[83] inkjet printing combined with vacuum-assisted thermal annealing was employed for scaling up. High-performance PSCs based on printed $MAPbI_3$ were demonstrated to obtain a PCE of 13.3% with an active area of 4.0 cm^2.[83] Recently, the emerging of all-inkjet-printed PSCs accelerates the process of industrialization. Hu *et al.*[80] fabricated a large-area (49 cm^2) PVK module that exhibited a PCE of 10.4% with a fully printable process. Besides, a 7 m^2 fully

printed PSC-based module has been successfully prepared (see Fig. 2c and d), showing promising potential in the practical photovoltaic application.

2.2 Vacuum based processes

As an alternative to solution-based processes, vacuum deposition has been explored to grow thin-film PVK from dry sources. There are two unique advantages of vacuum-based process. Firstly, the process does not involve the use of toxic solvents which may have a negative effect on the environment. The second advantage is the conformal growth onto rough substrates allowing, for example, the use of textured substrates in devices to improve light in-coupling.[84] This opens the integration of PVK cells on textured c-Si bottom cells for further applications.[85–87]

2.2.1 Thermal evaporation. In the thermal evaporation process, the precursor materials are sublimated by heating under high vacuum conditions. They are deposited onto substrates to form different material layers as shown in Fig. 3a. Therefore, this approach to fabricate PVK layers is scalable. According to the evaporation temperature of different source materials, a PVK film can be grown using two methods: co-evaporation[88,89] and sequential vacuum deposition.[90] Liu *et al.*[89] firstly reported PSCs with high PCEs, which were prepared by the dual-source co-evaporation method. Large area PVKs have also been reported. Borchert *et al.*[91] applied the co-evaporation method for large-area PVK deposition. Formamidinium lead triiodide ($FAPbI_3$) thin films were obtained with an area of 64 cm^2, as shown in Fig. 3b. Up to now, $MAPbI_3$ layer deposited by thermal evaporation demonstrates a PCE of 18.13% with 21 cm^2 active area (mini-modules).[92] However, a challenge for PVK deposition with thermal evaporation is the control of reaction between lead iodide (PbI_2) and MAI. The introduction of MAI may have an influence on chamber pressure, which will lead to fluctuations of the evaporation rate.[93] Therefore, hybrid approaches and multi-source depositions can be applied for PVK fabrication to avoid the MAI-induced chamber pressure fluctuations.[94,95] Feng *et al.*[96] successfully deposited some superior FA-based PVK films using low temperature annealing under vacuum. Compared with other solution based methods, thermal evaporation has been demonstrated to allow PVK deposition onto textured substrates,[97] and this feature provides a promising future for further applications. Sahli *et al.*[97] applied the sequential two-step method to deposit the PVK layer for a monolithic tandem device. The PVK film fully covered the μm-sized silicon pyramids (see Fig. 3c and d), and the tandem device achieved an efficiency as high as 25.2%.[97] Following the same approach, the same group demonstrated a PVK/PVK/c-Si monolithic triple-junction solar cell.[94] All-vacuum-processable PSCs are also obtained recently,[98,99] Lei *et al.* reported an all-evaporation method to achieve PCEs beyond 13% with an active area of 16 cm^2.[100] The recently reported improved results

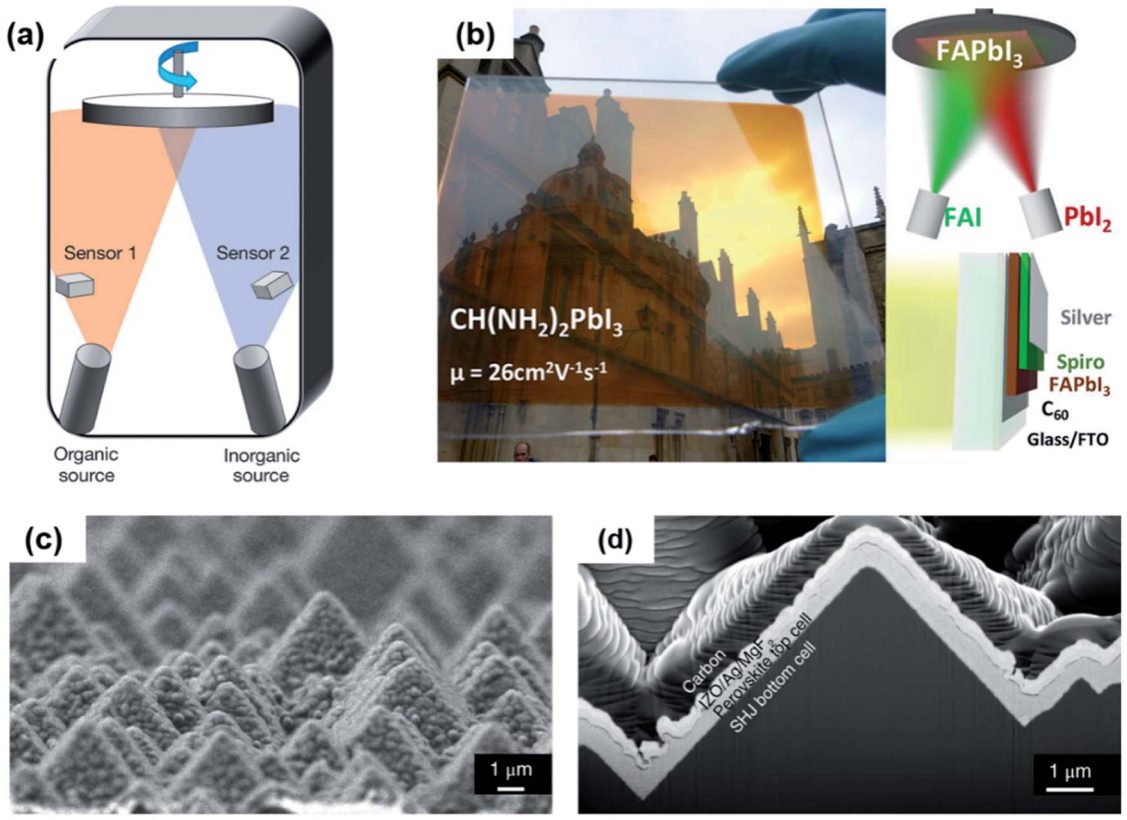

Fig. 3 (a) Schematic diagram of the co-evaporation of PVK film;[89] (b) image of 64 cm^2 $FAPbI_3$ thin film and corresponding fabrication process;[91] (c) SEM image of the PVK film fully covering the silicon pyramids;[97] (d) a cross-section of the PVK/SHJ monolithic tandem solar cell.[97]

based on thermal evaporation indicate the potential application in PSCs scaling up, especially for scalability and the compatibility with textured device-Si bottom cells.

2.2.2 Pulsed laser deposition. Pulsed laser deposition (PLD) is a versatile technique for stoichiometric deposition of various inorganic materials independently of vapour pressure to form thin films. The PLD configuration and deposition process are shown in Fig. 4a. Different from other vacuum-based approaches, PLD exhibits stoichiometric mass transfer of materials from the target to the substrate.[101] This unique advantage offers a potential application for PVK film formation. PLD consists of two main stages, namely formation of the target plasma and material deposition. In the first stage, the focused laser strikes the surface of the target material for a short time, ablating material that forms a so-called plasma plume containing ions and atoms. In the second stage, these excited ions directly impinge the substrate in front of the target. Film properties can be optimized by controlling the laser parameters,[102] substrate temperature,[102] and chamber pressure.[103] The first deposition of $MAPbI_3$ film based on PLD was reported by Bansode *et al.*[103] in 2015. Following the same method, they successfully deposited PVK films on silicon showing good crystal quality. The corresponding SEM-based top view and cross-sectional images are shown in Fig. 4b and c,[103] respectively. From then on, several PLD-grown inorganic metal halide PVKs have been successfully prepared, showing good photovoltaic properties and film stability.[104–106] Wang *et al.*[104] fabricated a dense $CsPbBr_3$ film *via* PLD. No significant decomposition was observed when the sample was placed in a highly humid (80%) environment for 15 days.[104] Lead-free PVK film formation is also achieved with PLD. $CsSnI_3$ film was recently reported by Kiyek *et al.*[105] The thickness-optimized film shows a stabilized black phase with a sharp absorption edge. About the deposition of organic–inorganic hybrid PVKs, another method named resonance infrared matrix-assisted pulsed laser evaporation[107] should be mentioned, showing low laser-induced damage of organic material. A detailed description of the new pulsed laser-based method can be found in Soto-Montero's review.[108] Based on the film quality as well as stability mentioned above, PLD has a potential application for scalable deposition of PVKs, especially in terms of fully inorganic PVK deposition.

2.3 Hybrid chemical vapor deposition

Hybrid chemical vapour deposition (HCVD) method can avoid solvent-related complications, which are challenging to control in industrial large-scale fabrication,[111] such as fast solvent removal and wettability issues. This method combines chemical vapour deposition (CVD) and other scalable deposition methods, such as thermal evaporation[112] or spray coating.[113] A typical PVK-based HCVD process consists of two steps: formation of inorganic film and organic/inorganic halide vapour deposition. The inorganic film is mainly deposited *via* thermal evaporation in reported works.[213,216] As for the CVD process, the organic halide vapour is optimized by pressure and temperature to deposit on the inorganic film, following a gas–solid reaction and converting into uniform PVK films.[114] The HCVD configuration and vapour deposition process for $MAPbI_3$ are shown in Fig. 4d. Several works have reported a successful formation of scalable PVK films by combining thermal evaporation and CVD.[109,110,115] Leyden *et al.*[109] firstly prepared a planar $MAPbCl_3$ device *via* HCVD method, achieving a PCE as high as 11.8%. Following the similar approach, Leyden *et al.*[110] again indicated the device upscaling process *via* HCVD. They fabricated $MAPbI_3$ based devices with a PCE of 9.5% (8.8 cm^2) and obtained a PCE of 9.0% (12 cm^2) for $FAPbI_3$ based devices, the corresponding up-scaling processes are shown in Fig. 4e. However, similarly to solution-based film formation, mixed-cations and mixed-halides play a critical role in film optoelectronic properties and stability.[115] Therefore, mixed cations/halides are commonly introduced in the first step by co-evaporation.[116] Differently

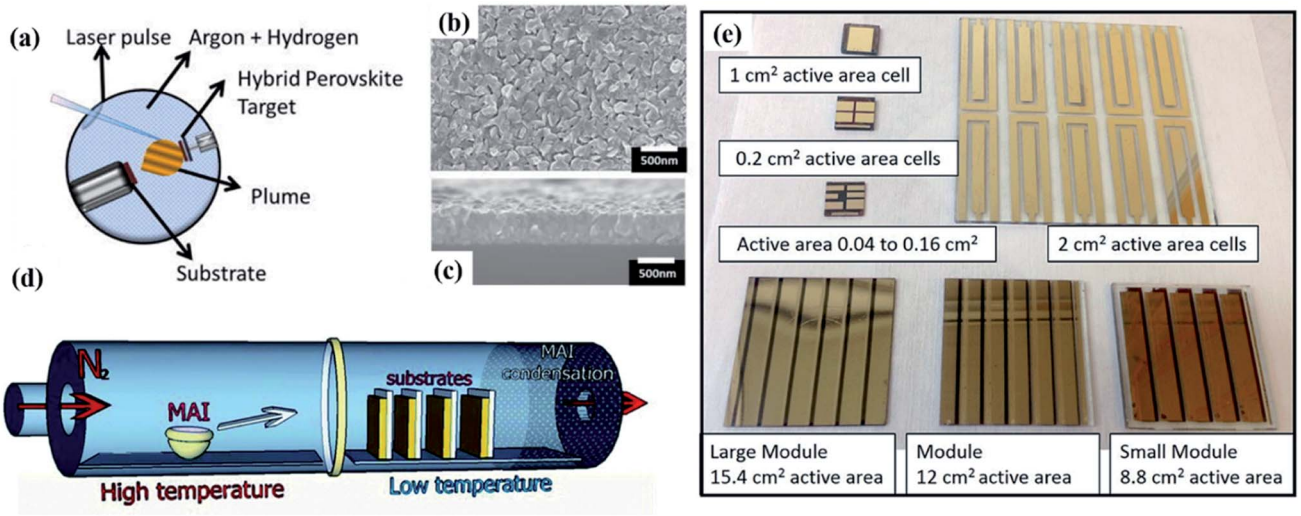

Fig. 4 (a) Schematic diagram of the PLD configuration and deposition process[103] (b) top view of PVK film on silicon wafer deposited with PLD[103] (c) the cross-section of the PLD PVK film[103] (d) schematic diagram of the HCVD configuration for MAI deposition onto PbI_2 coated substrates[109] (e) image of cells and modules prepared with HCVD approach demonstrating the up-scaling process.[110]

from this approach, Luo *et al.*[112] prepared a mixed-cation PVK film by optimizing the second step. They replaced pure FAI vapour with FAI/FACl mixed vapour to optimize the vapour–solid reaction, resulting in improved phase stability. Consequently, the large-sized PSC modules (active area of 41.25 cm^2) demonstrated champion PCE of 12.24%.

3. Challenges for device upscaling

The abovementioned deposition techniques are all for large area PVK film formation. As for other methods (*e.g.* CVD, soft-cover deposition), detailed technical parameters and models can be found somewhere else.[113,116–118] The device PCEs, deposition approaches, and corresponding areas are summarized in Fig. 5, which clearly shows that PCEs significantly decrease for large device areas. Therefore, the upscaling of PVK PV technology still faces challenges toward commercialization. In this section, we review the most significant challenges for processing high PCE devices from lab-scale to fab-scale.

3.1 Precursors and absorber layer

Upscaling of PVK films emphasizes the suitable storage of precursors as well as film deposition process. For solution-based methods, the precursor solution ratio and storage may have impacts on film quality, influencing both the nucleation and the crystal growth. To address this question, many attempts have been performed to control the film morphology and photovoltaic performance starting from a non-stoichiometric precursor solution.[143,144] As an example, excess of PbI_2 can lead to higher PCEs suggesting that unreacted PbI_2 improves the crystallinity of PVK films.[145] The reported precursor engineering may have some differences based on different solution deposition methods, but most of them are related to introducing of additives as stabilizer or mixing solvents to optimize the precursor viscosity as well as boiling point.[146] Table 1 briefly shows the reported requirements, approaches and corresponding solution-based deposition methods. Besides, the detailed PVK precursor solution chemistry is reviewed by Jung *et al.*[147] from fundamentals to industrialization.

Compared with solution-based methods, vacuum deposition can exactly control the deposited amount. However, one of the drawbacks is the lack of compatibility with additive engineering, which is an excellent approach to improve crystal quality, as shown in Table 2. Furthermore, this method shows less flexibility in the number of sources that can be incorporated in the final PVK material. For the deposition process, one of the most challenging part is to form a suitable interaction between substrate and precursors for both solution and vacuum related deposition approaches.[166] A better interaction not only depresses formation of non-radiative centres in the interfacial, but also has an influence on PVK crystal growth.

3.2 Charge transporting layers

For large area film fabrication, charge transporting layers (CTLs) should not only have appropriate energy alignment, thickness as well as conductivity, but also be suitable for scalable deposition. Furthermore, environmental stability, energy/time consumption, and costs, are also important aspects for up-scaling. Therefore, the selection of compatible materials and processes is important for PSC commercialization. In this section, CTLs will be briefly discussed focusing on challenges for both hole transporting layer (HTL) and electron transporting layer (ETL).

3.2.1 HTL. Organic materials, such as spiro-MeOTAD[171,172] and poly(triarylamine) (PTAA),[173,174] are widely used as hole transporting material for high-performance PSCs. Spiro-

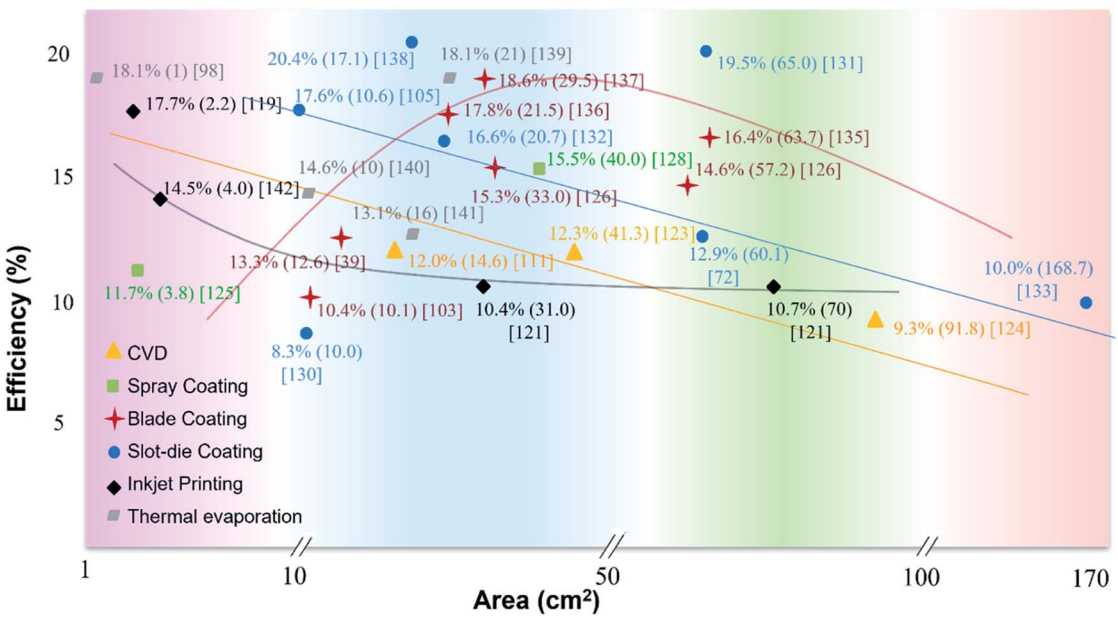

Fig. 5 Summary of PCEs as a function of the device area for PSCs prepared by different fabrication methods.[39,57,72,80,83,98,111,113,119–122,122–142]

Table 1 Different requirements and strategies of precursor solution preparation/storage based on different solution-based methods

Methods	Requirements	Approaches
Blade coating	Purified organic precursor[148] High viscosity[39]	Reductant[149,150] Moisture barrier[151] Material with synergistic effects[152]
Spray coating	Low viscosity[147] Suitable boiling point solvent[51]	Co-solvents[153] Low ink concentrations[54,154] Material with synergistic effects[155]
Slot die coating	—	Co-solvents[156–158] Lewis base additive[71] Material with synergistic effects[134,159,160]
Inkjet printing	Slow solvent evaporation[161]	Material with synergistic effects[82,162–164] Co-solvents[165]

Table 2 Comparison of solution- and vacuum-based depositions

	Advantages	Disadvantages
Solution methods	• Simple • Compatible with additive engineering[167]	• Solvent usage[168] • Low material utilization[169]
Vacuum methods	• Uniformity control on large area • Non-toxic solvent • Flexibility in substrate usage (low processing temperature)[170]	• limitation in number of sources evaporated • Long deposition process

MeOTAD is the most common HTL material in lab-scale device preparation. There are some successful examples for large area device preparation with spiro-MeOTAD as HTL. Luo *et al.*[112] prepared PVK solar modules with spiro-MeOTAD, the device achieved a PCE of 12.24% and device area is 64 cm^2. Following the spin coating method, Yang *et al.*[39] demonstrated a four-cell module (12.6 cm^2) with a stabilized efficiency output of 13.3%. Nevertheless, these pure organic HTL materials have low hole mobility, and dopants such as bis(trifluoromethane) sulfonimide lithium salt (LiTFSI) are required to improve the device PCE. Unfortunately, the introduction of the dopants can accelerate the degradation of PVK. Therefore, spiro-MeOTAD still has a gap between lab and fab due to its cost and the negative effect of dopant. In terms of inorganic materials, such as metal oxides, they are utilized not only to improve device stability but also to simplify the deposition process in mass production. Nickel oxide (NiO_x) is a popular HTL with high material stability.[175] NiO_x film can be formed with a variety of approaches, such as screen printing,[176] spin-coating,[177] and spray deposition.[178] However, the carrier mobility in NiO_x is also not so high and the reported NiO_x based device area is only 3–5 cm^2.[179,180]. Another commonly used metal oxide is molybdenum oxide (MoO_x).[181] Different MoO_x film morphologies are obtained with different approaches, such as solution preparation,[182] thermal evaporation,[183] blade coating,[184] and electrodeposition.[185] Thermally deposited MoO_x is commonly used in PSCs to realize energy level alignment and hole extraction.[186,187] It is generally applied together with spiro-MeOTAD as a bilayer because the interface reaction between MoO_x and PVK may accelerate the degradation of PVK.[188] Several other inorganic materials are also researched for HTL application, for example, CuSCN[189] and VO_x.[190,191] Even though small area devices based on CuSCN and VO_x have achieved excellent PV properties, PCEs drop dramatically with the increase of device area. Next to the abovementioned materials used as HTL in PSCs, some novel materials (such as TaTm:F_6-TCNNQ, TaTm) are also applied as HTL and the details can be found in ref. 192. Taking the cost and stability into consideration, inorganic materials show potential candidates for large area devices, further works focused on good film quality with high hole mobility should be achieved in near future.

3.2.2 ETL. SnO_2,[112,116] C_{60},[91,183] and PCBM[193,194] are most frequently used as ETLs for high PCE devices because of their high carrier mobility and excellent conductivity. Those materials can also be used for large area ETL fabrication. For TiO_2,[80,195,196] several works show outstanding properties.[197,198] Keremane *et al.*[198] printed in ambient atmosphere mesoporous TiO_2 enabling 11.55% PCE (70 cm^2). However, TiO_2 is reported to show a photocatalytic effect which may degrade the PVK absorber layer.[199] Atomic layer deposition (ALD)-based SnO_2 is also an excellent candidate demonstrating high V_{oc}, small J–V hysteresis, and negligible photocatalytic effect. Currently, the highest PCE of SnO_2-based PSCs has achieved 23.3% with an active area of 0.1 cm^2.[200] However, SnO_2-based large-area device fabrication still needs to be further improved, because SnO_2 has a higher probability of pinhole formation during film fabrication compared with TiO_2.[116] SnO_2 film needs to be thin while it is not easy to fully cover the substrate surface with extremely thin SnO_2 film. This problem is more critical for large area PSCs. Therefore, a trade-off between thickness and mobility needs to be carefully found. Up to now, the most successful example for SnO_2 film scaling up is by Qi's group.[116] By precise interface engineering, they demonstrated a PCE of 10% with a designated area of 91.8 cm^2.[116] PCBM is also applied for scalable deposition, which is usually in combination with other materials such as C_{60} or BCP to form an efficient electron transporting

bilayer.[134,193,194] Especially, C_{60} and BCP can be deposited by thermal evaporation, that makes these films easy to realize also on large area substrates, making it compatible with industrialization. The reported C_{60} and BCP based devices show PCEs of 14.6% (57.2 cm^2)[29] and 16.4% (63.7 cm^2).[135]

3.3 Back electrode

Thermally or e-beam evaporated metals (Au, Ag, Al) are the mostly used materials for the back electrode in PSCs. Analogous to the metal electrode in c-Si solar cells, a scalable and industrial process for metallization is a critical aspect to address in terms of material consumption for large-area devices. Cheaper materials are needed in replacement of noble metals when looking into commercialization. Nickel (Ni) film is also applied as back electrode for scalable PVK application.[201] One interesting aspect is that degraded PVK can be washed off from a device with Ni electrodes and then fresh PVK can be reloaded.[201] This unique recycling technology shows a new way for further development of low-cost PSCs. Besides, the direct contact between a metal and the CTL or PVK may lead to additional reactions. To address this issue, TCO films (for example, indium-doped tin oxide (ITO), aluminum-doped zinc oxide (AZO), indium-doped zinc oxide (IZO)) can be inserted between metal and CTL to prevent the undesired ion immigration. Lee *et al.*[202] fabricated large-scale PVK solar modules with application of multi-layered transparent electrodes, demonstrating excellent thermal stability. Carbon has also been proposed as electrode due to several advantages, such as high stability, low cost, excellent conductivity, and environmental protection.[203,204] A large-area (70 cm^2) PVK solar module with carbon electrode was fabricated, achieving a PCE of 10.74% (certified PCE 9.11%).[64] Besides, graphene is also an excellent candidate as electrode due to its good conductivity, stability and transparency.[205,206] Thus, it is commonly applied as electrode for PSC, especially for semi-transparent PSCs[207,208] or flexible PSCs.[209,210] Based on the above discussion, carbon electrodes show a potential application in PSC commercialization, especially because of their stability and low cost.

3.4 Stability of large area PVK devices

For commercialization of PSCs, device stability is a critical factor that should be taken into consideration, since long-term applications require that PSCs must be stable enough to continuously operate under outdoor conditions. However, PVK materials are sensitive to temperature, light, and humidity, leading to material decomposition and ion migration,[211] finally resulting in poor device stability. This part will highlight the potential instability of PSCs and strategies on the way towards industrialization.

3.4.1 Sources of instability. The instability of PVK and degradation mechanisms have been systematically studied based on experiments and simulations.[21,212] Lab-scale devices show improved stability *via* different optimization steps, such as introducing inorganic cations,[111,213] surface modification and using 2-dimensional (2D) materials.[214–216] However, to make PVK competitive to c-Si, the issues related to device lifetime still need to be addressed. The instability of PVK film comes mainly from defects (ion migration),[217,218] pinholes (lattice deformation),[219] and phase transition,[220] which may accelerate the degradation in presence of water,[221] high temperature,[222] light[223] and electric field.[224] To estimate the potential lifetime of PSCs, the International Electrotechnical Commission (IEC) is normally used based on a series of strict tests, such as UV-light, thermal cycling and damp heating.[142] The long-term operation of PSCs does not only depend on stability of PVK film, but also properties of CTLs and electrode, for example, the thermal instability of spiro,[225] UV-instability of TiO_2 (ref. 226) and reaction between I^- and Ag.[227]

3.4.2 Developments and strategies on long term device stability. Focusing on the instability problems mentioned in section 3.4.1, some strategies are proposed to improve the stability of large area PSCs, which can be summarized into four main parts. Firstly, component engineering. Inorganic cations such as Cs^+ and Rb^+ are introduced to stabilize the PVK cubic phase.[228,229] Secondly, interfacial modification is useful to not only passivate non-radiative central defects, increase resistance to moisture, but also hinder I^- migration.[230] As an example, the use of 2D materials has been successfully extended to large-area PSC fabrication.[231] It was reported that 2D material-based large-area PVK solar modules (PCE 13.4% for 108 cm^2 and 15.3% for 82 cm^2) showed excellent stability under thermal stress test at 65 °C (ISOSD2) for over 1000 h.[215] Thirdly, select other functional layer materials to replace susceptible CTLs and electrodes. Especially for the HTL, inorganic candidates such as NiO_x,[232] CuO_x[233] and CuSCN[234] are introduced to substitute organic materials. Table 3 summarizes the structure, stability, and corresponding performance of PSCs with areas larger than 5 cm^2. Finally, encapsulation. It is the final step of device fabrication, which provides a physical barrier protecting against various outdoor environmental factors. The company Microquanta Semiconductor announced that their encapsulated PVK

Table 3 The structure (light entering from the left-hand side), performance, and stability of large area (≥5.00 cm^2) PSCs

Structure	PCE (%)	Area (cm^2)	Stability	Ref.
Glass/ITO/NiO_x/PVK/Nb_2O_5/Ag	11.20	5.00	98% for 150 min, N_2 glove box, 100 °C	180
Glass/FTO/TiO_2/PVK/spiro-MeOTAD/Au	14.60	12.00	96% for 1200 min, steady-state measurement by tracking the MPP in N_2	111
Glass/FTO/d-TiO_2/m-TiO_2/PVK/WBH/P_3HT/Au	16.00	24.97	85% for 1370 h, RH 85%, room temperature	35
Glass/FTO/c-TiO_2/m-TiO_2/ZrO_2/PVK/carbon	10.40	49.00	30 days for RH 80%, 30 °C	80
Glass/FTO/c-TiO_2/m-TiO_2/ZrO_2/PVK/carbon	10.75	70.00	95% 2000 h, RH 65–70%, *T* 25–30 °C	243
Glass/FTO/c-TiO_2/m-TiO_2/ZrO_2/PVK/carbon	6.40	100.00	96% for full sun light illumination at 35 °C, 1046 h	244

module (20 cm^2) showed degradation of less than 2% after a 100 kW h ultraviolet (UV) preconditioning test (6.5 times IEC standards).[235] One thing need to be noted, we can observe a great variety of test conditions reported in the literature which makes a systematic comparison difficult. To solve this issue, a consensus statement[236] was given by many researchers for stability assessment. Based on the International Summit on Organic Photovoltaic Stability (ISOS) protocols, some other properties of PSCs are investigated, such as ion redistribution under electric fields, reversible degradation, and distinguishing ambient-induced degradation from other stress factors.[236] This section has a summary about strategies on PSC stability towards commercialization, the corresponding detailed information can be found in ref. 142, 237 and 238–242.

4. Scaling up of two-terminal monolithic tandem devices

To overcome the SQ limit of single-junction solar cells, the multijunction (MJ) configuration has been developed. The MJ approach is certainly not new in the PV community. In fact, it has been intensively investigated for thin-film Si[245–257] and III-V PV technologies.[258–266] It consists of two or more sub-cells that absorb light of different energies. By tuning the bandgap (E_g) of these sub-cells, better utilization of solar photons can be achieved resulting in higher PCEs. The simplest example is a so-called 'tandem' device consisting of two sub-cells stacked one on top of the other with engineered absorber layers. In the monolithic configuration, also known as two-terminal (2T), the sub-cells are electrically connected in series, meaning that the absorber properties must be carefully designed for 'current matching', namely each sub-cell should deliver an equal photocurrent. There are also other configurations, such as the four-terminal (4T),[267] which eliminates the current matching requirement and provides only a mechanical stacking, and the three-terminal (3T),[268] which is suitable for back-contacted bottom cell architectures.[269,270]

In this context, PVK/c-Si tandem device attracts much attention because of the stable and mature c-Si technology, the bandgap compatibility between the two absorbers, and the low processing temperature of the PVK top cell. Starting from the 1.12 eV of the E_g of c-Si and using a PVK top cell of 1.70 eV, the theoretical limit of PCE for PVK/c-Si monolithic tandem device is 44.1%.[271] Considering the great variety of PVK compositions and the ease of integration of new elements in the PVK lattice, E_g can be varied in a wide range of energies from 1.2 eV (ref. 272) to 3.0 eV.[273,274] Consequently, MJ solar cells fully consisting of PVK devices[30–32] or combinations with CIGS bottom cells[275–277] have been demonstrated. Independent of the deployed hybrid technologies, MJ devices using PVKs have shown a rapid PCE increase which can contribute to the acceleration towards the commercialization of PVK devices.

This section focuses on progress and challenges for PCE and stability, which is based on large area (≥1 cm^2) PVK/c-Si two-terminal monolithic tandem devices. The detailed discussion based on material, technical and device levels of small area PVK/c-Si tandem devices can be found somewhere else.[278–282]

4.1 Conversion efficiency

The efficiency of tandem devices is related to the properties of bottom cell, top cell, and various anti-reflective, recombination,

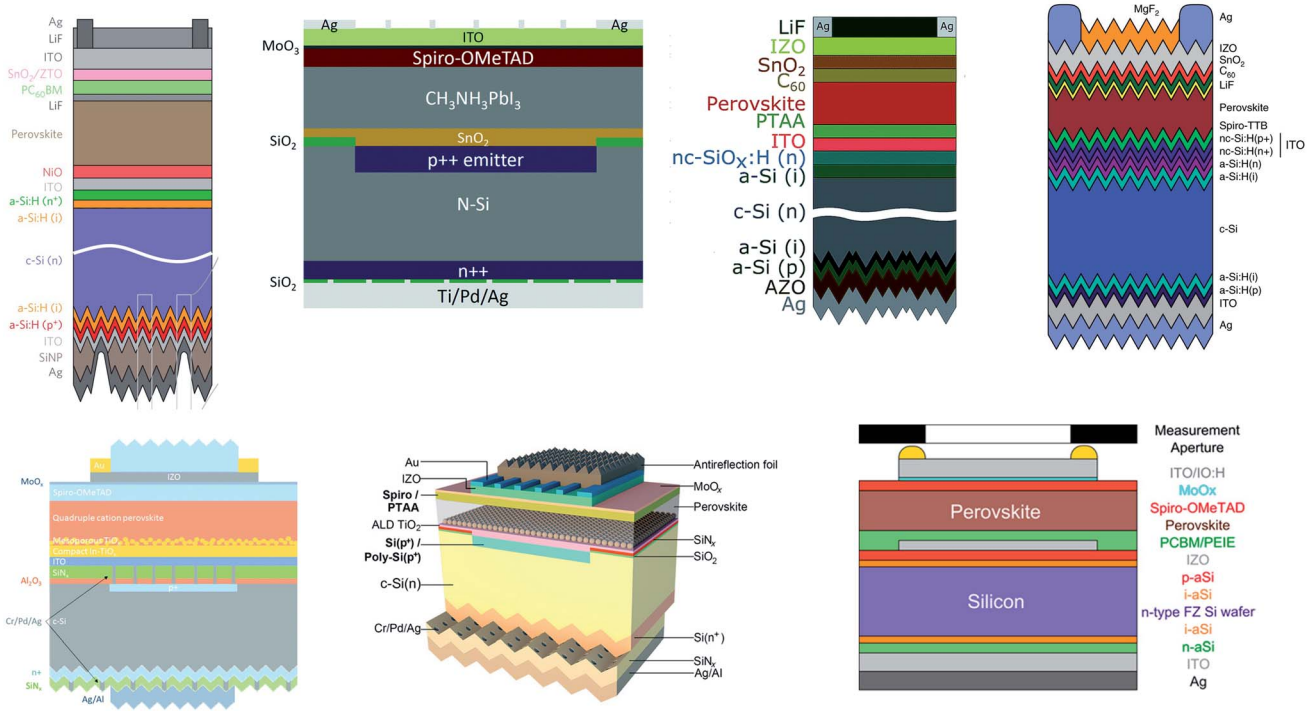

Fig. 6 A summary of different 2T tandem structures for large area PVK-based tandem devices.[31,97,285,289–293]

and contact layers. Homojunction and heterojunction silicon (SHJ) can be used as the bottom cell for both 4T[283,284] and 2T tandem devices.[97,285] SHJ solar cells are commonly chosen due to their high V_{oc} and PCE, which have a positive effect on the tandem device performance. Homojunction cells are also excellent candidates because they currently dominate most parts of the PV market. Up to now, works reported on efficiency improvement of large area tandem devices can be classified into three areas: PVK sub-cell optimization, recombination layer optimization and optical design. Fig. 6 shows a summary of different tandem structures, which were reported to be used for large area tandem devices.

4.1.1 PVK sub-cell. For 2T large area tandem solar cells, the PVK film quality strongly determines the top cell photovoltaic properties. It is a big challenge to form high-quality large area PVK film on a textured surface to enable integration with industry-relevant textured c-Si bottom cells. Hou *et al.*[286] demonstrated a solution processed PVK top cell with fully textured c-Si bottom cell by employing an μm-thick PVK layer.[286] In recent work, a two-step sequential vacuum process was applied for PVK deposition on textured surface.[287] Consequently, 100 cm^2 textured silicon substrate was perfectly covered by a PVK film *via* sputtering and CVD. In addition, interface modification, as well as composition engineering, have a huge influence on the whole device efficiency. Low-temperature (70 °C) slot-die coating was applied with a combination of modification strategy for top cell preparation.[288] A PVK/textured silicon monolithic 2T tandem device achieved a PCE of 23.8% with an area of 1 cm^2.[288] Besides, Cs^+ and FA^+ were also applied to tune the PVK bandgap and high device stability was obtained. The mixed-cation based PVK/c-Si solar cell achieved a PCE of 23.6% with an area of 1 cm^2.[289] Current matching cannot be ignored to obtain a high PCE for tandem device, and the most common method is to optimize the bandgap of the top cell. The bandgap optimization can be realized by composition engineering.

4.1.2 Recombination layer. Improvements in PCE are also driven by selection and optimization of the recombination layer between the two sub-cells. A thorough analysis of many aspects related to the recombination junction for tandem devices was recently published by Bastiani *et al.*[294] Most commonly, transparent conductive oxide (TCO) materials are used as recombination layers because they can fulfill both optical and electrical interconnection requirements. Up to now, recombination layers such as ITO, IZO, AZO have been generally applied for large area 2T tandem devices and excellent outcomes have been obtained. With optimization of the IZO thickness, Werner *et al.*[290] achieved a stable PCE of 19.2% over an aperture area of 1.22 cm^2. A PCE of 22.6% (area 57.4 cm^2) was achieved with a sputtered ITO recombination layer.[295] Apart from TCO layers, doped hydrogenated nanocrystalline silicon (nc-Si:H) has also been employed as a recombination layer. For example, Sahli *et al.*[97] introduced a nc-Si:H recombination junction to the tandem device with an effective decrease of the parasitic absorption and optical reflection, demonstrating a certified PCE of 25.2% with an active area of 1.419 cm^2.[97] Following a similar approach, PCE of 18.0% and 25.1% were obtained with areas of 12.96 cm^2 and 1.42 cm^2, respectively.[296] The use of nc-Si:H as the recombination layer for large area monolithic tandem devices has been mainly reported by EPFL until now. Another unique structure was reported by Zheng *et al.*:[291] the tandem device shows a recombination contact between SnO_2 and a p-doped region, as illustrated in Fig. 6. Compared with the common structure with an interfacial layer, SnO_2 serves not only as an ETL for the top cell, but also a recombination contact with the n-type silicon homojunction solar cell. As a result, PCEs of 17.6% (area 16.00 cm^2) and 21% (area 4.00 cm^2) were achieved.[291]

4.1.3 Optical design. Optical design is an efficient approach to further improve the device's short current density (J_{sc}) and to achieve current matching. Currently, optical design for PVK-based tandem devices deals with three aspects: (i) light trapping, (ii) reflection losses, and (iii) parasitic absorption.[297] Regarding light trapping, a rear-side textured bottom cell can effectively improve light trapping and increase its near-infrared spectral response.[298] In addition, textured structures can also be applied for light management at the front side of tandem devices.[290,299,300] As an example, Jošt *et al.*[301] employed a textured foil on the planar front-side of a tandem solar cell, significantly improving J_{sc} from 17.3 mA cm^{-2} to 18.5 mA cm^{-2}. As for the reduction of reflection losses, introducing an optical interlayer between the sub-cells can significantly decrease the reflection losses resulting from large differences in optical refractive index of Si and PVK. Mazzarella *et al.*[302] employed hydrogenated nanocrystalline silicon oxide (nc-SiO_x:H) with optimized refractive index and thickness as an optical interlayer of a tandem device resulting in 1.4 mA cm^{-2} current gain with a device area of 1 cm^2. Besides, nc-Si:H replacing ITO as a recombination layer improves the optical properties of monolithic tandem device,[296] shown in Fig. 6. Based on comparison with ITO, the nc-Si:H recombination junction was demonstrated to mitigate reflection at the sub-cell interface and increase the light transmittance to the bottom cell, consequently, the bottom cell photocurrent increased by more than 1 mA cm^{-2}.[296] In addition, thinner front ITO can also improve light-harvesting due to a lower parasitic absorption as well as reflection. Focussing on decreasing parasitic absorption, spectrum down-conversion materials can convert high energetic photons into visible light, which can be used to avoid the parasitic absorption of CTLs for tandem devices. Zheng *et al.*[303] employed $(Ba,Sr)_2SiO_4:Eu^{2+}$ phosphor at the front of the monolithic tandem cells to realize PCE as high as 23.1% for an area of 4 cm^2. It should be noted that J_{sc} has been dramatically improved from 14.1 mA cm^{-2} to 16.5 mA cm^{-2}. Besides, a thinner transparent electrode and inorganic HTL can effectively decrease the parasitic absorption and further improve the device J_{sc}. Current progress in terms of parameters and properties of PVK-based large area 2T tandem devices are summarized in Table 4.

4.2 Stability of large area PVK-based monolithic tandem devices

Currently, there are some works based on the stability of large-area monolithic tandem devices. The stability of PVK-based

Table 4 Parameters and properties of PVK-based large area 2T tandem devices. Reported results are sorted by date

PVK/silicon								
Silicon	Perovskite	Top cell bandgap (eV)	Recombination layer	Efficiency (%)	Area (cm^2)	Institute	Year	Ref.
Homo-junction	$MAPbI_3$	1.55	n^{++}/p^{++} Si	13.7	1.00	MIT/ stanford	2015	304
	$MAPbI_3$	1.55	ZTO	16.3	1.43	EPFL/CSEM	2016	305
	$CsRbFAMAPbI_{3-x}Br_x$	1.62	ITO	22.5	1.00	ANU	2017	292
	$MAPbI_3$	1.58	—	21.0	4.00	UNSW	2018	291
	$MAPbI_3$	1.58	—	17.6	16.00	UNSW	2018	291
	$(FAPbI_3)_{0.83}(MAPbBr_3)_{0.17}$	1.59	—	21.8	16.00	UNSW	2018	291
	$CsRbFAMAPbI_{3-x}Br_x$	1.62	—	23.2	1.00	ANU	2018	285
	$FAMAPbI_{3-x}Br_x$	1.61	—	23.1	4.00	UNSW	2019	303
SHJ	$MAPbI_3$	1.55	IZO	19.2	1.22	EPFL/CSEM	2015	290
	$MAPbI_3$	1.55	IZO	20.5	1.43	EPFL/CSEM	2016	283
	$CsFAPbI_{3-x}Br_x$	1.63	ITO	23.6	1.00	Stanford/ ASU	2017	289
	$CsFAPbI_{3-x}Br_x$	1.63	nc-Si:H	21.2	1.43	EPFL/CSEM	2017	296
	$CsFAPbI_{3-x}Br_x$	1.63	nc-Si:H	18.0	12.96	EPFL/CSEM	2017	296
	$CsFAPbI_{3-x}Br_x$	1.63	nc-Si:H	25.2	1.419	EPFL/CSEM	2018	97
	$CsRbFAMAPbI_{3-x}Br_x$	1.62	—	24.1	1.00	ANU	2018	285
	$CsFAPbI_{3-x}Br_x$	1.68	ITO	25.0	1.00	Stanford/ ASU	2018	300
	$CsFAPbI_{3-x}Br_x$	1.63	nc-Si:H	25.4	1.43	EPFL	2019	306
	$Cs_{0.05}(FA_{0.77}MA_{0.23})_{0.95}Pb(I_{0.77}Br_{0.23})_3$	1.68	ITO	29.1	1.06	HZB	2020	307
	$(FA_{0.65}MA_{0.2}Cs_{0.15})Pb(I_{0.8}Br_{0.2})_3$	1.68	ITO	26.2	1.00	KAIST	2020	308
	$FA_{0.75}Cs_{0.25}Pb(I_{0.8}Br_{0.2})_3$	1.67	ITO	27.1	1.00	CU-Boulder	2020	309
	$(Cs_{0.06}FA_{0.78}MA_{0.16})Pb(Br_{0.17}I_{0.83})_3$	1.64	ITO	26.3	1.43	C.H.O.S.E	2020	310
	$Cs_xFA_{1-x}PbI_yBr_{1-y}$	1.63	ITO	22.6	57.4	CSEM/EPFL	2019	295
	$MAPb(I_{0.75}Br_{0.25})_3$	1.68	ITO	23.8	1.00	KSC	2020	288

monolithic tandem devices is mainly determined by the PVK sub-cell. c-Si is stable enough to operate consistently for many years in ambient conditions. Therefore, the research based on large-area tandem device stability is mainly focused on the top-cell stability improvement. According to recent studies, pinholes are among the factors responsible for device instability. The existence of pinholes leads to film instability because of a decrease in carrier lifetime and mobility.[308] To solve this problem, Bush *et al.*[289] applied a bilayer SnO_2/ZTO by ALD or pulsed-CVD deposition to prevent the formation of pinholes. The double-layer enables the device to withstand a 1000 hour damp heat test at 85 °C and 85% relative humidity. Another factor is the reaction between the electrode (Ag) and halogens in PVK. Reducing the reaction between PVK and the Ag electrode can also improve the device stability.[309] Sahli *et al.*[97] pointed out that buffer layers, as well as a transparent conductive electrode, can efficiently prevent ion migration and suppress the reaction of PVK with the Ag electrode. Besides, a stable carbon or gold electrode can largely improve the device's stability. A third factor impacting stability is moisture/light/temperature-induced environmental degradation. Inorganic materials can be applied to improve thermal stability, such as Cs^+ for PVK[289] and NiO_x for the HTL. As for molecular water, dense buffer layers or transparent polymer layers are introduced to realize a moisture barrier.[97,303] In addition, spectrum down-conversion materials are employed to transfer high-energy photons into low energy photons, realizing a device UV stability.[303] Table 5 summarizes the large area device stabilities in detail. Compared to c-Si solar cells, the stability of PVK-based large area 2T tandem solar cells still needs to be improved further.

Table 5 Summary of stability for large area PVK-based 2T tandem devices sorted per device area from the smallest to the largest

Structure	PCE (%)	Area (cm^2)	Stability	Ref.
$CsFAPbI_{3-x}Br_x$PVK/SHJ	23.6	1.00	80% for 1000 h, 85% RH, 85 °C	289
$FA_{0.75}Cs_{0.25}Pb(I_{0.8}Br_{0.2})_3$PVK/SHJ	27.1	1.00	96% for 1000 hours of MPP operation at 60 °C.	309
$Cs_5(MA_{17}FA_{83})_{95}Pb(I_{83}Br_{17})_3$PVK/CIGS	23.3	1.03	97% for 11 h, 40 °C, under constant illumination at MPP	311
$CsFAPbI_{3-x}Br_x$PVK/SHJ	25.2	1.42	90% after 270 hours under constant illumination at MPP	97
$FAMAPbI_{3-x}Br_x$PVK/homojunction	23.1	4.00	90% for 288 h, UV exposure	303
$(FAPbI_3)_{0.83}(MAPbBr_3)_{0.17}$PVK/homojunction Si	21.8	16.00	91%, for 31 days, room temperature, N_2	312

5. Other issues

5.1 Costs

PVK holds the potential for low-cost production due to the use of abundant material, low processing temperature, and simple deposition methods. The cost of modules is estimated to be around 2 US$ m^{-2}.[313] Therefore, the potentially low cost of PSCs has drawn a lot of attention in the PV market. However, the total industrialization costs, especially when the materials, the life-cycle, and energy consumption are taken into consideration, still don't have a conclusive assessment yet. This section will give a brief illustration of the industrialization cost, focusing on manufacturing cost and levelized cost of energy (LCOE).

5.1.1 Manufacturing cost. The processing cost of PVK solar modules is estimated to be 6.8 ± 1.2 US$ m^{-2} based on fully printed devices with sputtering TCO and Al electrode,[314] while the processing costs of CIGS and CdTe modules are 29 and 27 US$ m^{-2}, respectively.[315,316] The costs mentioned above exclude the price of glass, frame, laminating film, junction-box, and testing. The lower costs for PVK solar modules originate from cheaper materials used and lower energy consumption. A detailed comparison between PVK and other PV materials for industrialization has been reported in ref. 317. About the material costs, Cai *et al.*[318] listed a comparison based on two representative examples of PSCs. The results are shown in Fig. 7a where the calculated costs for materials of module A (expensive example) was 0.127 US$ W^{-1}, which was higher than that of module B (cheap example) of 0.102 US$ W^{-1}. For both examples, the highest expense among the materials comes from the TCO, while the cost of the PVK layer is minor. For the processing costs, Chang *et al.*[319] performed a detailed cost distribution of all steps for PVK solar modules based on a fully printing method, as shown in Fig. 7b. Once again, TCO fabrication accounts for a large part of the fabricating cost.

Cost modelling is also applied to analyse the PVK/silicon tandem PV technology. Efficiency potential and cost evaluation are accessed in terms of tandem devices and modules. Based on six demonstrated tandem structures, Chang *et al.*[320] found that the cost barriers are in PVK part because of the expensive transporting layer materials. In particular, the use of homojunction cells with p-type wafers helps to decrease the total costs. With similar approach, Messmer *et al.*[321] has an assessment on both PCEs (optical and electrical) and costs based on four promising silicon bottom cell concepts. The detailed comparison between these structures is shown in ref. 321. All these tandem-based cost analysis points out that attentions should be directed to cheaper materials and feasible techniques in the recent future.

5.1.2 Levelized cost of energy. PV techno-economic competitiveness can be evaluated by the LCOE value. Compared with silicon solar cells,[322] PSCs still exhibit a higher LCOE because of their high capital expenditure. It is a big challenge for PSC fabrication to reach similar costs as silicon solar cells with a similar size, especially considering that the price of silicon drastically reduced over the last 39 years.[322] The relationship between LCOE, PCE and lifetime based on PVK solar modules has been discussed by Song *et al.*[314] and Cai *et al.*[318] The LCOE values ranging from 4.93 to 7.90 ¢ kW^{-1} h^{-1} when device can operate with a PCE of 16% for around 30 years.[314] Fig. 7c summarizes the LCOE for PVK PV modules with different PCEs and lifetimes. The module lifetime strongly affects the value of LCOE. Under the condition that modules

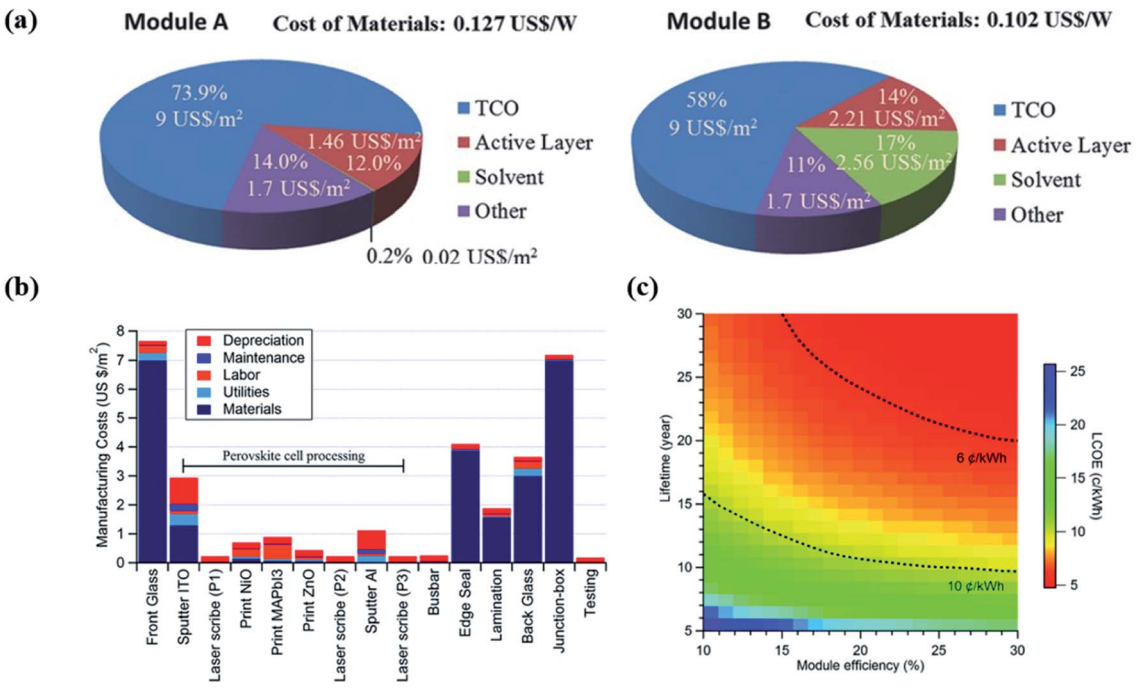

Fig. 7 (a) Material cost analysis for two representative examples[318] (b) cost contribution of each step for PVK solar modules manufacturing process.[319] (c) The relationship between PCE, lifetime, and LCOE for PVK PV modules.[314]

work constantly, the LCOE are 10 ¢ kW^{-1} h^{-1} and 6 ¢ kW^{-1} h^{-1} assuming different lifetimes of 10 years and around 23 years, respectively.[314] Therefore, stability improvement is an important factor for industrialization of modules related to ambient stability and encapsulation.

The LCOE of PVK/silicon tandem modules is also evaluated, normally together with a detailed comparison of silicon and PVK single junction in reported works.[323] By applying this approach, Zafoschnig *et al.*[324] find that PVK/silicon tandem devices have a promising application if the module has a long lifetime and the PCE can exceed 30% using low-cost industrial-scale processes in the next 5–6 years.[324] Therefore, the short lifetime of PSCs (compared to more than 25 years for silicon solar cells) and low-cost processing should be especially addressed in near future.[325,326]

5.2 Perovskite solar cell reproducibility

Although many PSC-related articles have reported high PCEs and excellent stabilities, these data are usually the best or average value over many cells. For the PSC industrialization, efforts based on large-area PVK fabrication need to overcome the reproducibility problem. For different fabrication techniques, device reproducibility is mentioned. Vapor-assisted growth method is indicated to have high reproducibility. Gujar *et al.*[327] demonstrated that 35 devices (36 in total) fabricated with vapor-assisted method worked with very little fluctuation of the photovoltaic parameters (V_{oc}, J_{sc}, FF and PCE). Following a similar method, Leyden *et al.*[328] and Borchert *et al.*[329] also achieved high device reproducibility for large-area PSCs. In addition, spray coating[56] and slot-die coating[134] have also been discussed in detail based on large-area PSC reproducibility. Apart from the active layer, the reproducibility of CTLs is also reported.[330] PSCs with e-beam evaporated NiO_x as HTL show high uniformity and reproducibility.[331] However, these studies emphasize the influence of the fabrication technique on reproducibility. Materials should also be taken into consideration for PSC fabrication. Odabası *et al.*[332] assessed the reproducibility by comparing a large number of PSCs using pooled variances (S_p^2) comparing different materials and methods. The S_p^2 parameters are graphically reported in Fig. 8 and classified by materials that are commonly used in PSCs.[332] The reproducibility is higher for lower S_p^2 values. This figure provides guidance for identifying the most promising materials for PVK in PV applications. For the ETL, compact SnO_2 is an excellent candidate compared with other materials. P3HT and PTAA show smaller S_p^2 values compared with spiro-MeOTAD when looking at the HTL. It should be noted that HTL-free devices have also smaller S_p^2 values when compared to inorganic HTLs for instance. For common electrode materials reported in this study, the use of carbon results in a higher device reproducibility.

5.3 Life cycle assessment

A life cycle assessment (LCA) is employed to evaluate the environmental profile and potential impact of PVK solar modules due to lead toxicity and fabrication exhaust.[333] A detailed relationship between PCE, stability and environmental impacts based on PSCs is systematically reviewed by A. Urbina.[334] In his work, the author reports different materials and configurations discussing the corresponding environmental impacts.[334] Ibn-Mohammed *et al.*[335] reported on the LCA of PVK solar modules based on $MAPbX_3$ and $CsFAPbX_3$. They provide a comparison of a PVK device to other existing PV technologies based on energy consumption, environmental profile and energy payback period (EPBP).[335] They pointed out that not only the toxicity of lead, but also the processing of the operating emissions and used materials should be taken into consideration when evaluating the impact on environment. Besides, greenhouse gas emissions factor (GEF) of the PSC, as well as OPV, are much higher than other PV technologies because of their short lifetime, shown in Fig. 9a.[335] Therefore, long-term stability indirectly affects energy consumption. In addition, a HTL-free device is also modelled providing excellent LCA results.[336] Fig. 9b shows the comparison of the PSCs with

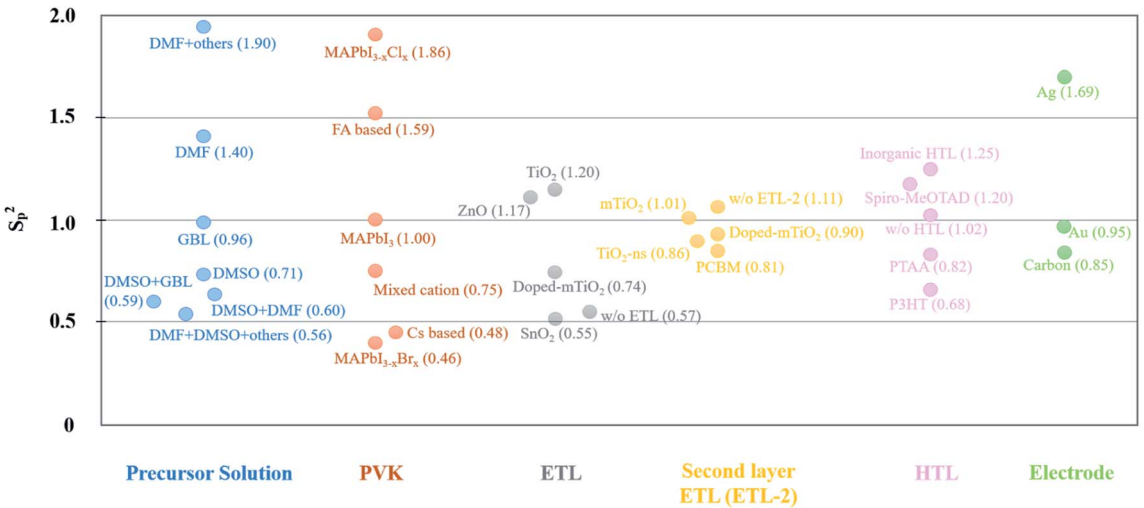

Fig. 8 The S_p^2 value of materials for each layer of PSCs. The data comes from ref. 332.

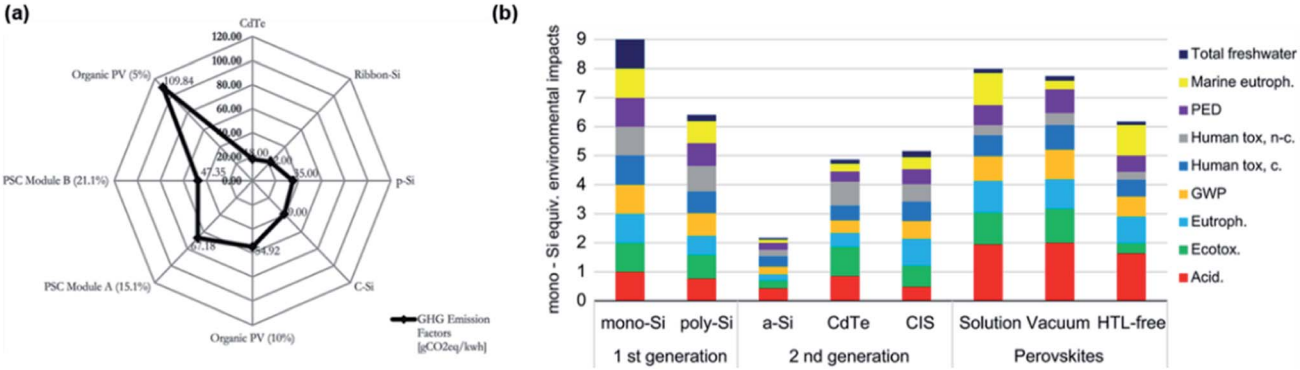

Fig. 9 (a) A comparison of GEF based on different PV technologies[335] (b) a comparison of environmental impacts based on different factors between PSC and other PV technologies.[336]

commercial PV technologies. Environmental impact of global warming potential and primary energy demand are shown as GWP and PED in Fig. 9b.

Moreover, a LCA of PVK-based tandem solar cells has also been modelled.[337–339] Tian *et al.*[340] performed a LCA on the EPBP, carbon footprint, and environmental impact scores for both PVK/silicon and PVK/PVK tandem devices. They emphasized that periodic module replacement and material recycling strategies should be implemented to accelerate the application of PVK/silicon tandem devices in PV market.[340] To avoid the trouble of module replacement, a method was proposed by Barkhouse *et al.*[341] in 2015. Their modelled results showed that it is important to maintain high infrared transparency and conductivity for the PVK layer after the top cell has stopped working. These properties could ensure that the underlying silicon cell can continue to work without requiring module replacement.[341] The detailed discussion and comparison of LCA on PVK/silicon and other single-junctions can be found in Leccisi's review.[342]

5.4 Summary of companies

With the rapid development towards PSC scaling up, a few companies have been focussing on module fabrication. Most of these companies aim to realize large-area devices (area >100 cm^2) mainly using screen printing,[235] roll-to-roll printing,[343] inkjet-printing[344] for the PVK film formation. Besides, some companies fabricate flexible PVK solar modules, such as Toshiba,[345] Saule Technologies[344] and Energy Materials Corporation.[343] Oxford PV has started a manufacturing line for PVK/c-Si tandem cells that are expected to commence production in the year 2021.[346] Detailed company information and corresponding progress are summarized in Table 6.

6. Conclusion and outlook

In this review, the developments and challenges for PSCs from lab-to-fab are systematically discussed focusing on different relevant aspects. In the past years, key material processing,

Table 6 Recent development of PSCs for institutions and companies

Company name	Country	Efficiency (%)	Area (cm^2)	Type of devices	Ref.
Oxford PV	United Kingdom	28.0	1	PVK/silicon tandem cells	346
		29.5	—	PVK/silicon tandem cells	352
HZB	Germany	29.8	1	PVK/silicon tandem cells	34
Greatcell solar	Australia	—	20	Focusing on the solar enablement of two substrates: glass and steel, 20 cm^2 PVK module	347
Weihua solar	China	10.6	25	PVK solar module, carbon electrode, HTL-free	348
Solliance solar research	Netherlands	14.5	144	PVK solar module	66
Microquanta semiconductor	China	17.9	227	PVK solar module	235
Solaronix	Switzerland	12.0	500	PVK solar module	349
Toshiba	Japan	11.7	703	PVK flexible solar module	345
Panasonic	Japan	16.1	802	PVK solar submodule (55 series cells)	350
Wonder solar	China	—	110×10^4 (3600 cm^2 for each module)	PVK PV system, screen-printed triple mesoscopic PVK solar modules	9
Saule Technologies	Poland	—	—	Inkjet-printed flexible PSCs	344
Energy materials Corporation	United States	—	—	High speed, roll-to-roll printing lines	343
Swift solar	United States	—	—	All-PVK tandem cells and modules	351

scalable device fabrication, and PSC properties have been investigated in depth. However, compared with other well-established PV technologies, both the efficiency and stability of PSCs show a large gap between small-area cells and large-area modules. To achieve the goals of PSCs upscaling and further industrialization, many issues need to be addressed, including not only the efficiency, but also stability, costs, reproducibility, and fabrication techniques. At present, the main challenges involving PSCs commercialization are: (1) long term stability. Modules should ensure durable outdoor operation under operative conditions such as long-term illumination and heat; (2) cost issues. More efforts should be devoted to identify alternative low-cost raw materials for each layer composing the cell, as well as simplifying the device process; (3) further applications. Broad the PSCs application market, for example, tandem device, flexible device, and indoor PV technology. Finally, we are still at the early stage of the PSCs industrialization. In the long term, can PVK realistically become a competitive candidate in the PV market to uptake silicon technology? How the research community will be able to come up with new ideas and solutions aiming at addressing the key challenges/problems we discussed in this review, will indicate the future paths, and define the success of the emerging PVK technology.

Conflicts of interest

There are no conflicts to declare.

References

1 C. Szeles, *Phys. Status Solidi B*, 2004, **241**, 783–790.
2 K. Yoshikawa, H. Kawasaki, W. Yoshida, T. Irie, K. Konishi, K. Nakano, T. Uto, D. Adachi, M. Kanematsu, H. Uzu and K. Yamamoto, *Nat. Energy*, 2017, **2**, 17032.
3 A. Richter, *et al.*, *10th Int. Conf. Cryst. Silicon Photovoltaics, Leuven, Belgium, Silicon PV*, 2020.
4 F. Haase, C. Hollemann, S. Schäfer, A. Merkle, M. Rienäcker, J. Krügener, R. Brendel and R. Peibst, *Sol. Energy Mater. Sol. Cells*, 2018, **186**, 184–193.
5 A. Kojima, K. Teshima, Y. Shirai and T. Miyasaka, *J. Am. Chem. Soc.*, 2009, **131**, 6050–6051.
6 N. R. E. L. (NREL), Best Research-Cell Efficiency Chart | Photovoltaic Research | NREL.
7 S. Agarwal and P. R. Nair, *J. Appl. Phys.*, 2017, **2**, 163104.
8 J. Yan, N. Li, Y. Ai, Z. Wang, W. Yang, M. Zhao, C. Shou, B. Yan, J. Sheng and J. Ye, *Sustainable Energy Fuels*, 2019, **3**, 3448–3454.
9 Y. Rong, Y. Hu, A. Mei, H. Tan, M. I. Saidaminov, S. Il Seok, M. D. McGehee, E. H. Sargent and H. Han, *Science*, 2018, **361**, 1214–1221.
10 G. Divitini, S. Cacovich, F. Matteocci, L. Cinà, A. Di Carlo and C. Ducati, *Nat. Energy*, 2016, **1**, 15012.
11 K. Domanski, E. A. Alharbi, A. Hagfeldt, M. Grätzel and W. Tress, *Nat. Energy*, 2018, **3**, 61–67.
12 J. Yang, B. D. Siempelkamp, D. Liu and T. L. Kelly, *ACS Nano*, 2015, **9**, 1955–1963.
13 M. Shirayama, M. Kato, T. Miyadera, T. Sugita, T. Fujiseki, S. Hara, H. Kadowaki, D. Murata, M. Chikamatsu and H. Fujiwara, *J. Appl. Phys.*, 2016, **119**, 115501.
14 R. K. Misra, S. Aharon, B. Li, D. Mogilyansky, I. Visoly-Fisher, L. Etgar and E. A. Katz, *J. Phys. Chem. Lett.*, 2015, **6**, 326–330.
15 X. Tang, M. Brandl, B. May, I. Levchuk, Y. Hou, M. Richter, H. Chen, S. Chen, S. Kahmann, A. Osvet, F. Maier, H. P. Steinrück, R. Hock, G. J. Matt and C. J. Brabec, *J. Mater. Chem. A*, 2016, **4**, 15896–15903.
16 J. Wei, Q. Wang, J. Huo, F. Gao, Z. Gan, Q. Zhao and H. Li, *Adv. Energy Mater.*, 2020, **2002326**, 35–37.
17 S. Sun, A. Tiihonen, F. Oviedo, Z. Liu, J. Thapa, Y. Zhao, N. T. P. Hartono, A. Goyal, T. Heumueller, C. Batali, A. Encinas, J. J. Yoo, R. Li, Z. Ren, I. M. Peters, C. J. Brabec, M. G. Bawendi, V. Stevanovic, J. Fisher and T. Buonassisi, *Matter*, 2021, **4**, 1–18.
18 T. A. Berhe, W. N. Su, C. H. Chen, C. J. Pan, J. H. Cheng, H. M. Chen, M. C. Tsai, L. Y. Chen, A. A. Dubale and B. J. Hwang, *Energy Environ. Sci.*, 2016, **9**, 323–356.
19 C. C. Boyd, R. Cheacharoen, K. A. Bush, R. Prasanna, T. Leijtens and M. D. McGehee, *ACS Energy Lett.*, 2018, **3**, 1772–1778.
20 J. Carolus, T. Merckx, Z. Purohit, B. Tripathi, H. G. Boyen, T. Aernouts, W. De Ceuninck, B. Conings and M. Daenen, *Sol. RRL*, 2019, **3**, 1–3.
21 C. C. Boyd, R. Cheacharoen, T. Leijtens and M. D. McGehee, *Chem. Rev.*, 2019, **119**, 3418–3451.
22 J. Li, J. Huang, A. Zhao, Y. Li and M. Wei, *J. Mater. Chem. C*, 2020, **8**, 8840–8845.
23 R. Chen, Y. Wu, Y. Wang, R. Xu, R. He, Y. Fan, X. Huang, J. Yin, B. Wu, J. Li and N. Zheng, *Adv. Funct. Mater.*, 2020, **2008760**, 1–8.
24 G. Tong, D. Y. Son, L. K. Ono, Y. Liu, Y. Hu, H. Zhang, A. Jamshaid, L. Qiu, Z. Liu and Y. Qi, *Adv. Energy Mater.*, 2021, **2003712**, 1–11.
25 J. Yang, Q. Hong, Z. Yuan, R. Xu, X. Guo, S. Xiong, X. Liu, S. Braun, Y. Li, J. Tang, C. Duan, M. Fahlman and Q. Bao, *Adv. Opt. Mater.*, 2018, **6**, 1–8.
26 M. C. Brennan, S. Draguta, P. V. Kamat and M. Kuno, *ACS Energy Lett.*, 2018, **3**, 204–213.
27 T. Leijtens, G. E. Eperon, N. K. Noel, S. N. Habisreutinger, A. Petrozza and H. J. Snaith, *Adv. Energy Mater.*, 2015, **5**, 1–23.
28 M. Jeong, I. W. Choi, E. M. Go, Y. Cho, M. Kim, B. Lee, S. Jeong, Y. Jo, H. W. Choi, J. Lee, J. H. Bae, S. K. Kwak, D. S. Kim and C. Yang, *Science*, 2020, **369**, 1615–1620.
29 Y. Deng, X. Zheng, Y. Bai, Q. Wang, J. Zhao and J. Huang, *Nat. Energy*, 2018, **3**, 560–566.
30 K. Xiao, J. Wen, Q. Han, R. Lin, Y. Gao, S. Gu, Y. Zang, Y. Nie, J. Zhu, J. Xu and H. Tan, *ACS Energy Lett.*, 2020, **5**, 2819–2826.
31 K. Xiao, R. Lin, Q. Han, Y. Hou, Z. Qin, H. T. Nguyen, J. Wen, M. Wei, V. Yeddu, M. I. Saidaminov, Y. Gao, X. Luo, Y. Wang, H. Gao, C. Zhang, J. Xu, J. Zhu, E. H. Sargent and H. Tan, *Nat. Energy*, 2020, **5**, 870–880.

32 J. Wang, V. Zardetto, K. Datta, D. Zhang, M. M. Wienk and R. A. J. Janssen, *Nat. Commun.*, 2020, **11**, 1–10.
33 W. Shockley and H. J. Queisser, *J. Appl. Phys.*, 1961, **32**, 510–519.
34 https://www.pv-magazine.com/2021/11/22/helmholtz-center-achieves-29-80-efficiency-for-perovskite-silicon-tandem-solar-cell/.
35 E. H. Jung, N. J. Jeon, E. Y. Park, C. S. Moon, T. J. Shin, T. Y. Yang, J. H. Noh and J. Seo, *Nature*, 2019, **567**, 511–515.
36 X. Dai, Y. Deng, C. H. Van Brackle, S. Chen, P. N. Rudd, X. Xiao, Y. Lin, B. Chen and J. Huang, *Adv. Energy Mater.*, 2020, **10**, 1–7.
37 J. Zhong, W. Wu, L. Ding and D. Kuang, *Energy Environ. Mater.*, 2021, **4**, 277–283.
38 S. Razza, F. Di Giacomo, F. Matteocci, L. Cinà, A. L. Palma, S. Casaluci, P. Cameron, A. D'Epifanio, S. Licoccia, A. Reale, T. M. Brown and A. Di Carlo, *J. Power Sources*, 2015, **277**, 286–291.
39 M. Yang, Z. Li, M. O. Reese, O. G. Reid, D. H. Kim, S. Siol, T. R. Klein, Y. Yan, J. J. Berry, M. F. A. M. Van Hest and K. Zhu, *Nat. Energy*, 2017, **2**, 1–9.
40 A. T. Mallajosyula, K. Fernando, S. Bhatt, A. Singh, B. W. Alphenaar, J. C. Blancon, W. Nie, G. Gupta and A. D. Mohite, *Appl. Mater. Today*, 2016, **3**, 96–102.
41 Y. Zhong, R. Munir, J. Li, M.-C. Tang, M. R. Niazi, D.-M. Smilgies, K. Zhao and A. Amassian, *ACS Energy Lett.*, 2018, **3**, 1078–1085.
42 M. C. Tang, Y. Fan, D. Barrit, X. Chang, H. X. Dang, R. Li, K. Wang, D. M. Smilgies, S. F. Liu, S. De Wolf, T. D. Anthopoulos, K. Zhao and A. Amassian, *J. Mater. Chem. A*, 2020, **8**, 1095–1104.
43 J. Li, R. Munir, Y. Fan, T. Niu, Y. Liu, Y. Zhong, Z. Yang, Y. Tian, B. Liu, J. Sun, D. M. Smilgies, S. Thoroddsen, A. Amassian, K. Zhao and S. (Frank) Liu, *Joule*, 2018, **2**, 1313–1330.
44 J. Yin, Y. Lin, C. Zhang, J. Li and N. Zheng, *ACS Appl. Mater. Interfaces*, 2018, **10**, 23103–23111.
45 J. H. Kim, S. T. Williams, N. Cho, C. C. Chueh and A. K. Y. Jen, *Adv. Energy Mater.*, 2015, **5**, 2–7.
46 N. G. Park and K. Zhu, *Nat. Rev. Mater.*, 2020, **5**, 333–350.
47 Z. Ouyang, M. Yang, J. B. Whitaker, D. Li and M. F. A. M. van Hest, *ACS Appl. Energy Mater.*, 2020, **3**, 3714–3720.
48 S. Chen, X. Dai, S. Xu, H. Jiao, L. Zhao and J. Huang, *Science*, 2021, **373**, 902–907.
49 C. Girotto, D. Moia, B. P. Rand and P. Heremans, *Adv. Funct. Mater.*, 2011, **21**, 64–72.
50 L. H. Chou, X. F. Wang, I. Osaka, C. G. Wu and C. L. Liu, *ACS Appl. Mater. Interfaces*, 2018, **10**, 38042–38050.
51 A. T. Barrows, A. J. Pearson, C. K. Kwak, A. D. F. Dunbar, A. R. Buckley and D. G. Lidzey, *Energy Environ. Sci.*, 2014, **7**, 2944–2950.
52 H. Chen, X. Ding, X. Pan, T. Hayat, A. Alsaedi, Y. Ding and S. Dai, *J. Power Sources*, 2018, **402**, 82–90.
53 H. Ishihara, S. Sarang, Y. C. Chen, O. Lin, P. Phummirat, L. Thung, J. Hernandez, S. Ghosh and V. Tung, *J. Mater. Chem. A*, 2016, **4**, 6989–6997.
54 M. Habibi, A. Rahimzadeh, I. Bennouna and M. Eslamian, *Coatings*, 2017, **7**, 42–57.
55 Y. S. Chou, L. H. Chou, A. Z. Guo, X. F. Wang, I. Osaka, C. G. Wu and C. L. Liu, *ACS Sustainable Chem. Eng.*, 2019, **7**, 14217–14224.
56 M. Park, W. Cho, G. Lee, S. C. Hong, M. C. Kim, J. Yoon, N. Ahn and M. Choi, *Small*, 2019, **15**, 1–7.
57 Z. Liang, S. Zhang, X. Xu, N. Wang, J. Wang, X. Wang, Z. Bi, G. Xu, N. Yuan and J. Ding, *RSC Adv.*, 2015, **5**, 60562–60569.
58 Z. Bi, Z. Liang, X. Xu, Z. Chai, H. Jin, D. Xu, J. Li, M. Li and G. Xu, *Sol. Energy Mater. Sol. Cells*, 2017, **162**, 13–20.
59 J. E. Bishop, J. A. Smith and D. G. Lidzey, *ACS Appl. Mater. Interfaces*, 2020, **12**, 48237–48245.
60 J. H. Heo, F. Zhang, C. Xiao, S. J. Heo, J. K. Park, J. J. Berry, K. Zhu and S. H. Im, *Joule*, 2021, **5**, 481–494.
61 D. K. Mohamad, J. Griffin, C. Bracher, A. T. Barrows and D. G. Lidzey, *Adv. Energy Mater.*, 2016, **6**, 1–7.
62 E. Bi, W. Tang, H. Chen, Y. Wang, J. Barbaud, T. Wu, W. Kong, P. Tu, H. Zhu, X. Zeng, J. He, S. I. Kan, X. Yang, M. Grätzel and L. Han, *Joule*, 2019, **3**, 2748–2760.
63 M. Fievez, P. J. Singh Rana, T. M. Koh, M. Manceau, J. H. Lew, N. F. Jamaludin, B. Ghosh, A. Bruno, S. Cros, S. Berson, S. G. Mhaisalkar and W. L. Leong, *Sol. Energy Mater. Sol. Cells*, 2021, **230**, 111189.
64 G. Cotella, J. Baker, D. Worsley, F. De Rossi, C. Pleydell-Pearce, M. Carnie and T. Watson, *Sol. Energy Mater. Sol. Cells*, 2017, **159**, 362–369.
65 Solliance, Solliance sets more world records for R2R perovskite solar cells and modules, https://www.solliance.eu/2017/solliance-sets-more-world-records-for-r2r-perovskite-solar-cells-and-modules/.
66 F. Di Giacomo, H. Fledderus, H. Gorter, G. Kirchner, I. De Vries, I. Dogan, W. Verhees, V. Zardetto, M. Najafi, D. Zhang, H. Lifka, Y. Galagan, T. Aernouts, S. Veenstra, P. Groen and R. Andriesse, *2018 IEEE 7th World Conf. Photovolt. Energy Conversion, WCPEC 2018-A Jt. Conf. 45th IEEE PVSC, 28th PVSEC 34th EU PVSEC*, 2018, pp. 2795–2798.
67 F. Xu, J. Liu, A. S. Subbiah, W. Liu, J. Kang, G. T. Harrison, X. Yang, F. H. Isikgor, E. Aydin, M. De Bastiani and S. De Wolf, *Small Sci.*, 2021, **1**, 2000044.
68 S. Bernard, S. Jutteau, S. Mejaouri, S. Cacovich, I. Zimmermann, A. Yaiche, S. Gbegnon, D. Loisnard, S. Collin, A. Duchatelet, F. Sauvage and J. Rousset, *Sol. RRL*, 2021, **5**, 1–10.
69 J. Wang, M. R. Squillante, S. Sidhik, A. Mohite and M. S. J. Marshall, *2021 IEEE 48th Photovoltaic Specialists Conference (PVSC)*, 2021, pp. 1128–1130.
70 I. Zimmermann, M. Al Atem, O. Fournier, S. Bernard, S. Jutteau, L. Lombez and J. Rousset, *Adv. Mater. Interfaces*, 2021, **8**, 1–9.
71 Z. Yang, W. Zhang, S. Wu, H. Zhu, Z. Liu, Z. Liu, Z. Jiang, R. Chen, J. Zhou, Q. Lu, Z. Xiao, L. Shi, H. Chen, L. K. Ono, S. Zhang, Y. Zhang, Y. Qi, L. Han and W. Chen, *Sci. Adv.*, 2021, **7**, 1–14.

72 M. Xu, W. Ji, Y. Sheng, Y. Wu, H. Cheng, J. Meng, Z. Yan, J. Xu, A. Mei, Y. Hu, Y. Rong and H. Han, *Nano Energy*, 2020, **74**, 1–8.
73 M. Mercuri, K. Pierpauli, M. G. Bellino and C. L. A. Berli, *Langmuir*, 2017, **33**, 152–157.
74 T. Bu, J. Li, H. Li, C. Tian, J. Su, G. Tong, L. K. Ono, C. Wang, Z. Lin, N. Chai, X. L. Zhang, J. Chang, J. Lu, J. Zhong, W. Huang, Y. Qi, Y. B. Cheng and F. Huang, *Science*, 2021, **372**, 1327–1332.
75 S. H. Huang, C. K. Guan, P. H. Lee, H. C. Huang, C. F. Li, Y. C. Huang and W. F. Su, *Adv. Energy Mater.*, 2020, **10**, 1–9.
76 K. Hwang, Y. S. Jung, Y. J. Heo, F. H. Scholes, S. E. Watkins, J. Subbiah, D. J. Jones, D. Y. Kim and D. Vak, *Adv. Mater.*, 2015, **27**, 1241–1247.
77 L. Gao, K. Huang, C. Long, F. Zeng, B. Liu and J. Yang, *Appl. Phys. A: Mater. Sci. Process.*, 2020, **126**, 1–7.
78 F. Di Giacomo, S. Shanmugam, H. Fledderus, B. J. Bruijnaers, W. J. H. Verhees, M. S. Dorenkamper, S. C. Veenstra, W. Qiu, R. Gehlhaar, T. Merckx, T. Aernouts, R. Andriessen and Y. Galagan, *Sol. Energy Mater. Sol. Cells*, 2018, **181**, 53–59.
79 R. Patidar, D. Burkitt, K. Hooper, D. Richards and T. Watson, *Mater. Today Commun.*, 2020, **22**, 100808.
80 Y. Hu, S. Si, A. Mei, Y. Rong, H. Liu, X. Li and H. Han, *Sol. RRL*, 2017, **1**, 2–7.
81 P. Li, C. Liang, B. Bao, Y. Li, X. Hu, Y. Wang, Y. Zhang, F. Li, G. Shao and Y. Song, *Nano Energy*, 2018, **46**, 203–211.
82 Z. Li, P. Li, G. Chen, Y. Cheng, X. Pi, X. Yu, D. Yang, L. Han, Y. Zhang and Y. Song, *ACS Appl. Mater. Interfaces*, 2020, **12**, 39082–39091.
83 C. Liang, P. Li, H. Gu, Y. Zhang, F. Li, Y. Song, G. Shao, N. Mathews and G. Xing, *Sol. RRL*, 2018, **2**, 1–9.
84 L. Gil-Escrig, M. Roß, J. Sutter, A. Al-Ashouri, C. Becker and S. Albrecht, *Sol. RRL*, 2021, **5**, 1–9.
85 L. Gil-Escrig, M. Roß, J. Sutter, A. Al-Ashouri, C. Becker and S. Albrecht, *Sol. RRL*, 2020, **2000553**, 1–9.
86 L. Cojocaru, K. Wienands, T. W. Kim, S. Uchida, A. J. Bett, S. Rafizadeh, J. C. Goldschmidt and S. W. Glunz, *ACS Appl. Mater. Interfaces*, 2018, **10**, 26293–26302.
87 P. S. C. Schulze, K. Wienands, A. J. Bett, S. Rafizadeh, L. E. Mundt, L. Cojocaru, M. Hermle, S. W. Glunz, H. Hillebrecht and J. C. Goldschmidt, *Thin Solid Films*, 2020, **704**, 137970.
88 C. Gao, J. Liu, C. Liao, Q. Ye, Y. Zhang, X. He, X. Guo, J. Mei and W. Lau, *RSC Adv.*, 2015, **5**, 26175–26180.
89 M. Liu, M. B. Johnston and H. J. Snaith, *Nature*, 2013, **501**, 395–398.
90 C.-W. Chen, H.-W. Kang, S.-Y. Hsiao, P.-F. Yang, K.-M. Chiang and H.-W. Lin, *Adv. Mater.*, 2014, **26**, 6647–6652.
91 J. Borchert, R. L. Milot, J. B. Patel, C. L. Davies, A. D. Wright, L. Martínez Maestro, H. J. Snaith, L. M. Herz and M. B. Johnston, *ACS Energy Lett.*, 2017, **2**, 2799–2804.
92 J. Li, H. Wang, X. Y. Chin, H. A. Dewi, K. Vergeer, T. W. Goh, J. W. M. Lim, J. H. Lew, K. P. Loh, C. Soci, T. C. Sum, H. J. Bolink, N. Mathews, S. Mhaisalkar and A. Bruno, *Joule*, 2020, **4**, 1035–1053.
93 S. Wang, X. Li, J. Wu, W. Wen and Y. Qi, *Curr. Opin. Electrochem.*, 2018, **11**, 130–140.
94 J. Werner, F. Sahli, F. Fu, J. J. Diaz Leon, A. Walter, B. A. Kamino, B. Niesen, S. Nicolay, Q. Jeangros and C. Ballif, *ACS Energy Lett.*, 2018, **3**, 2052–2058.
95 L. Gil-Escrig, C. Dreessen, F. Palazon, Z. Hawash, E. Moons, S. Albrecht, M. Sessolo and H. J. Bolink, *ACS Energy Lett.*, 2021, **6**, 827–836.
96 J. Feng, Y. Jiao, H. Wang, X. Zhu, Y. Sun, M. Du, Y. Cao, D. Yang and S. F. Liu, *Energy Environ. Sci.*, 2021, **14**, 3035–3043.
97 F. Sahli, J. Werner, B. A. Kamino, M. Bräuninger, R. Monnard, B. Paviet-Salomon, L. Barraud, L. Ding, J. J. Diaz Leon, D. Sacchetto, G. Cattaneo, M. Despeisse, M. Boccard, S. Nicolay, Q. Jeangros, B. Niesen and C. Ballif, *Nat. Mater.*, 2018, **17**, 820–826.
98 M. M. Tavakoli and R. Tavakoli, *Phys. Status Solidi RRL*, 2021, **15**, 1–8.
99 Y. Choi, D. Koo, M. Jeong, G. Jeong, J. Lee, B. Lee, K. J. Choi, C. Yang and H. Park, *Sol. RRL*, 2021, **5**, 1–10.
100 T. Lei, F. Li, X. Zhu, H. Dong, Z. Niu, S. Ye, W. Zhao, J. Xi, B. Jiao, L. Ding and Z. Wu, *Sol. RRL*, 2020, **2000292**, 1–9.
101 H. M. Christen and G. Eres, *J. Phys.: Condens. Matter*, 2008, **20**, 264005–264021.
102 S. Hoffmann-Urlaub, Y. Zhang, Z. Wang, B. Kressdorf and T. Meyer, *Appl. Phys. A: Mater. Sci. Process.*, 2020, **126**, 1–11.
103 U. Bansode and S. Ogale, *J. Appl. Phys.*, 2017, **121**, 0021–8979.
104 H. Wang, Y. Wu, M. Ma, S. Dong, Q. Li, J. Du, H. Zhang and Q. Xu, *ACS Appl. Energy Mater.*, 2019, **2**, 2305–2312.
105 V. M. Kiyek, Y. A. Birkhölzer, Y. Smirnov, M. Ledinsky, Z. Remes, J. Momand, B. J. Kooi, G. Koster, G. Rijnders and M. Morales-Masis, *Adv. Mater. Interfaces*, 2020, **7**, 5–9.
106 W. A. Dunlap-Shohl, Y. Zhou, N. P. Padture and D. B. Mitzi, *Chem. Rev.*, 2019, **119**, 3193–3295.
107 R. Pate and A. D. Stiff-Roberts, *Chem. Phys. Lett.*, 2009, **477**, 406–410.
108 T. Soto-Montero, W. Soltanpoor and M. Morales-Masis, *APL Mater.*, 2020, **8**, 110903.
109 M. R. Leyden, L. K. Ono, S. R. Raga, Y. Kato, S. Wang and Y. Qi, *J. Mater. Chem. A*, 2014, **2**, 18742–18745.
110 M. R. Leyden, Y. Jiang and Y. Qi, *J. Mater. Chem. A*, 2016, **4**, 13125–13132.
111 Y. Jiang, M. R. Leyden, L. Qiu, S. Wang, L. K. Ono, Z. Wu, E. J. Juarez-Perez and Y. Qi, *Adv. Funct. Mater.*, 2018, **28**, 1703835.
112 L. Luo, Y. Zhang, N. Chai, X. Deng, J. Zhong, F. Huang, Y. Peng, Z. Ku and Y. B. Cheng, *J. Mater. Chem. A*, 2018, **6**, 21143–21148.
113 Y. Jiang, M. Remeika, Z. Hu, E. J. Juarez-Perez, L. Qiu, Z. Liu, T. Kim, L. K. Ono, D. Y. Son, Z. Hawash, M. R. Leyden, Z. Wu, L. Meng, J. Hu and Y. Qi, *Adv. Energy Mater.*, 2019, **9**, 1–12.
114 X. Liu, L. Cao, Z. Guo, Y. Li, W. Gao and L. Zhou, *Materials*, 2019, **12**, 1–17.
115 L. Liu, A. Mei, X. Li, H. Han, Y. Dkhissi, A. D. Scully, R. A. Caruso, Y. B. Cheng, I. Jeong, J. Lee, M. J. Ko, K. Yong, B.

S. Richards, T. L. Kelly, N. Pellet, M. Levi and S. Turri, Research|reports, 354, 2016.
116 L. Qiu, S. He, Y. Jiang, D. Y. Son, L. K. Ono, Z. Liu, T. Kim, T. Bouloumis, S. Kazaoui and Y. Qi, *J. Mater. Chem. A*, 2019, **7**, 6920–6929.
117 H. Chen, F. Ye, W. Tang, J. He, M. Yin, Y. Wang, F. Xie, E. Bi, X. Yang, M. Grätzel and L. Han, *Nature*, 2017, **550**, 92–95.
118 F. Ye, H. Chen, F. Xie, W. Tang, M. Yin, J. He, E. Bi, Y. Wang, X. Yang and L. Han, *Energy Environ. Sci.*, 2016, **9**, 2295–2301.
119 P. Li, C. Liang, B. Bao, Y. Li, X. Hu, Y. Wang and Y. Zhang, *Nano Energy*, 2018, **46**, 203–211.
120 Z. Li, P. Li, G. Chen, Y. Cheng, X. Pi, X. Yu, D. Yang, L. Han, Y. Zhang and Y. Song, *ACS Appl. Mater. Interfaces*, 2020, **12**, 39082–39091.
121 A. Priyadarshi, L. J. Haur, P. Murray, D. Fu, S. Kulkarni, G. Xing, T. C. Sum, N. Mathews and S. G. Mhaisalkar, *Energy Environ. Sci.*, 2016, 3687–3692.
122 M. R. Leyden, Y. Jiang and Y. Qi, *J. Mater. Chem. A*, 2016, **4**, 13125.
123 L. Luo, Y. Zhang, N. Chai, X. Deng, J. Zhong, F. Huang, Y. Peng, Z. Ku and Y. B. Cheng, *J. Mater. Chem. A*, 2018, **6**, 21143–21148.
124 L. Qiu, S. He, Y. Jiang, D. Son, L. K. Ono, Z. Liu, T. Kim, T. Bouloumis, S. Kazaoui and Y. Qi, *J. Mater. Chem. A*, 2019, **7**, 6920–6929.
125 C. A. M. De Huerta, U. W. Paetzold, R. Gehlhaar, D. Cheyns and P. Heremans, *J. Mater. Chem. A*, 2016, **4**, 3792–3797.
126 Y. Deng, X. Zheng, Y. Bai, Q. Wang, J. Zhao and J. Huang, *Nat. Energy*, 2018, **3**, 560–566.
127 H. Huang, J. Shi, L. Zhu, D. Li, Y. Luo and Q. Meng, *Nano Energy*, 2016, **27**, 352–358.
128 S. Hyuk, *J. Mater. Chem. A*, 2016, **4**, 17636.
129 L. Cai, L. Liang, J. Wu, B. Ding, L. Gao and B. Fan, *J. Semicond.*, 2017, **38**, 014006.
130 D. Lee, Y. Jung, Y. Heo, S. Lee, K. Hwang and Y. Jeon, *ACS Appl. Mater. Interfaces*, 2018, **10**, 16133–16139.
131 D. Vak, K. Hwang, A. Faulks, Y. S. Jung, N. Clark, D. Y. Kim, G. J. Wilson and S. E. Watkins, *Adv. Energy Mater.*, 2015, **5**, 1–8.
132 Z. Yang, W. Zhang, S. Wu, H. Zhu, Z. Liu, Z. Liu, Z. Jiang, R. Chen, J. Zhou, Q. Lu, Z. Xiao, L. Shi, H. Chen, L. K. Ono, S. Zhang, Y. Zhang, Y. Qi, L. Han and W. Chen, *Sci. Adv.*, 2021, **7**, 1–14.
133 F. Di, S. Shanmugam, H. Fledderus, B. J. Bruijnaers, W. J. H. Verhees, M. S. Dorenkamper, S. C. Veenstra and W. Qiu, *Sol. Energy Mater. Sol. Cells*, 2018, **181**, 53–59.
134 D. Lee, Y. S. Jung, Y. J. Heo, S. Lee, K. Hwang, Y. J. Jeon, J. E. Kim, J. Park, G. Y. Jung and D. Y. Kim, *ACS Appl. Mater. Interfaces*, 2018, **10**, 16133–16139.
135 Y. Deng, C. H. van Brackle, X. Dai, J. Zhao, B. Chen and J. Huang, *Sci. Adv.*, 2019, **5**, 1–9.
136 Y. Deng, Z. Ni, F. Axel and X. Xiao, *Joule*, 2020, **4**, 1949–1960.
137 Y. Deng, S. Xu, S. Chen, X. Xiao, J. Zhao and J. Huang, *Nat. Energy*, 2021, **6**, 633–641.
138 T. Bu, J. Li, H. Li, C. Tian, J. Su, G. Tong, L. K. Ono, C. Wang, Z. Lin, N. Chai, X. Zhang, J. Chang, J. Lu, J. Zhong, W. Huang, Y. Qi, Y. Cheng and F. Huang, *Science*, 2021, **372**, 1327–1332.
139 J. Li, H. Wang, X. Yu, J. Li, H. Wang, X. Y. Chin, H. A. Dewi, K. Vergeer and T. W. Goh, *Joule*, 2020, **4**, 1035–1053.
140 J. Feng, Y. Jiao, H. Wang, X. Zhu, Y. Sun, M. Du, Y. Cao, D. Yang and S. F. Liu, *Energy Environ. Sci.*, 2021, **14**, 3035–3043.
141 T. Lei, F. Li, X. Zhu, H. Dong, Z. Niu, S. Ye, W. Zhao, J. Xi, B. Jiao, L. Ding and Z. Wu, *Sol. RRL*, 2020, **2000292**, 1–9.
142 Z. Yang, S. Zhang, L. Li and W. Chen, *J Materiomics.*, 2017, **3**, 231–244.
143 Y. Rong, S. Venkatesan, R. Guo, Y. Wang, J. Bao, W. Li, Z. Fan and Y. Yao, *Nanoscale*, 2016, **8**, 12892–12899.
144 G. Longo, A. Wong, M. Sessolo and H. J. Bolink, *J. Lumin.*, 2017, **189**, 120–125.
145 C. Roldán-Carmona, P. Gratia, I. Zimmermann, G. Grancini, P. Gao, M. Graetzel and M. K. Nazeeruddin, *Energy Environ. Sci.*, 2015, **8**, 3550–3556.
146 D. H. Kim, J. B. Whitaker, Z. Li, M. F. A. M. van Hest and K. Zhu, *Joule*, 2018, **2**, 1437–1451.
147 M. Jung, S. G. Ji, G. Kim and S. Il Seok, *Chem. Soc. Rev.*, 2019, **48**, 2011–2038.
148 Y. Deng, E. Peng, Y. Shao, Z. Xiao, Q. Dong and J. Huang, *Energy Environ. Sci.*, 2015, **8**, 1544–1550.
149 Q. Wang, M. Eslamian, T. Zhao and A. K. Y. Jen, *IEEE J. Photovoltaics*, 2018, **8**, 1662–1669.
150 S. Chen, X. Xiao, H. Gu and J. Huang, *Sci. Adv.*, 2021, **7**, 1–7.
151 W. Q. Wu, Z. Yang, P. N. Rudd, Y. Shao, X. Dai, H. Wei, J. Zhao, Y. Fang, Q. Wang, Y. Liu, Y. Deng, X. Xiao, Y. Feng and J. Huang, *Sci. Adv.*, 2019, **5**, 1–10.
152 Z. Xu, R. Chen, Y. Wu, R. He, J. Yin, W. Lin, B. Wu, J. Li and N. Zheng, *J. Mater. Chem. A*, 2019, **7**, 26849–26857.
153 J. Su, H. Cai, J. Yang, X. Ye, R. Han, J. Ni, J. Li and J. Zhang, *ACS Appl. Mater. Interfaces*, 2020, **12**, 3531–3538.
154 J. E. Bishop, T. J. Routledge and D. G. Lidzey, *J. Phys. Chem. Lett.*, 2018, **9**, 1977–1984.
155 J. H. Heo, M. H. Lee, M. H. Jang and S. H. Im, *J. Mater. Chem. A*, 2016, **4**, 17636–17642.
156 J. Li, J. Dagar, O. Shargaieva, M. A. Flatken, H. Köbler, M. Fenske, C. Schultz, B. Stegemann, J. Just, D. M. Többens, A. Abate, R. Munir and E. Unger, *Adv. Energy Mater.*, 2021, **11**, 2003460.
157 Y. Galagan, F. Di Giacomo, H. Gorter, G. Kirchner, I. de Vries, R. Andriessen and P. Groen, *Adv. Energy Mater.*, 2018, **8**, 1–7.
158 D. Burkitt, R. Patidar, P. Greenwood, K. Hooper, J. McGettrick, S. Dimitrov, M. Colombo, V. Stoichkov, D. Richards, D. Beynon, M. Davies and T. Watson, *Sustainable Energy Fuels*, 2020, **4**, 3340–3351.
159 G. Cotella, J. Baker, D. Worsley, F. De Rossi, C. Pleydell-Pearce, M. Carnie and T. Watson, *Sol. Energy Mater. Sol. Cells*, 2017, **159**, 362–369.
160 D. Burkitt, R. Swartwout, J. McGettrick, P. Greenwood, D. Beynon, R. Brenes, V. Bulović and T. Watson, *RSC Adv.*, 2019, **9**, 37415–37423.
161 F. Mathies, T. Abzieher, A. Hochstuhl, K. Glaser, A. Colsmann, U. W. Paetzold, G. Hernandez-Sosa,

U. Lemmer and A. Quintilla, *J. Mater. Chem. A*, 2016, **4**, 19207–19213.
162 C. Zuo, D. Vak, D. Angmo, L. Ding and M. Gao, *Nano Energy*, 2018, **46**, 185–192.
163 L. Zhang, S. Chen, X. Wang, D. Wang, Y. Li, Q. Ai, X. Sun, J. Chen, Y. Li, X. Jiang, S. Yang and B. Xu, *Sol. RRL*, 2021, **5**, 1–11.
164 A. Giuri, E. Saleh, A. Listorti, S. Colella, A. Rizzo, C. Tuck and C. E. Corcione, *Nanomaterials*, 2019, **9**, 582–594.
165 B. Dou, J. B. Whitaker, K. Bruening, D. T. Moore, L. M. Wheeler, J. Ryter, N. J. Breslin, J. J. Berry, S. M. Garner, F. S. Barnes, S. E. Shaheen, C. J. Tassone, K. Zhu and M. F. A. M. Van Hest, *ACS Energy Lett.*, 2018, **3**, 2558–2565.
166 L. Qiu, S. He, L. K. Ono, S. Liu and Y. Qi, *ACS Energy Lett.*, 2019, **4**, 2147–2167.
167 D. K. Lee, K. S. Lim, J. W. Lee and N. G. Park, *J. Mater. Chem. A*, 2021, **9**, 3018–3028.
168 M. Zhang, D. Xin, X. Zheng, Q. Chen and W. H. Zhang, *ACS Sustainable Chem. Eng.*, 2020, **8**, 13126–13138.
169 Y. Vaynzof, *Adv. Energy Mater.*, 2020, **10**, 2003073.
170 C. Roldán-Carmona, O. Malinkiewicz, A. Soriano, G. Mínguez Espallargas, A. Garcia, P. Reinecke, T. Kroyer, M. I. Dar, M. K. Nazeeruddin and H. J. Bolink, *Energy Environ. Sci.*, 2014, **7**, 994–997.
171 M. H. Li, C. W. Hsu, P. S. Shen, H. M. Cheng, Y. Chi, P. Chen and T. F. Guo, *Chem. Commun.*, 2015, **51**, 15518–15521.
172 Z. Hawash, L. K. Ono and Y. Qi, *Adv. Mater. Interfaces*, 2018, **5**, 1700623.
173 D. Luo, W. Yang, Z. Wang, A. Sadhanala, Q. Hu, R. Su, R. Shivanna, G. F. Trindade, J. F. Watts, Z. Xu, T. Liu, K. Chen, F. Ye, P. Wu, L. Zhao, J. Wu, Y. Tu, Y. Zhang, X. Yang, W. Zhang, R. H. Friend, Q. Gong, H. J. Snaith and R. Zhu, *Science*, 2018, **360**, 1442–1446.
174 M. M. Tavakoli and R. Tavakoli, *Phys. Status Solidi RRL*, 2020, **2000449**, 2000449.
175 A. C. Nkele, A. C. Nwanya, N. M. Shinde, S. Ezugwu, M. Maaza, J. S. Shaikh and F. I. Ezema, *Int. J. Energy Res.*, 2020, **44**, 9839–9863.
176 K. Cao, Z. Zuo, J. Cui, Y. Shen, T. Moehl, S. M. Zakeeruddin, M. Grätzel and M. Wang, *Nano Energy*, 2015, **17**, 171–179.
177 X. Yin, M. Que, Y. Xing and W. Que, *J. Mater. Chem. A*, 2015, **3**, 24495–24503.
178 W. J. Scheideler, N. Rolston, O. Zhao, J. Zhang and R. H. Dauskardt, *Adv. Energy Mater.*, 2019, **9**, 1–8.
179 T. Abzieher, S. Moghadamzadeh, F. Schackmar, H. Eggers, F. Sutterlüti, A. Farooq, D. Kojda, K. Habicht, R. Schmager, A. Mertens, R. Azmi, L. Klohr, J. A. Schwenzer, M. Hetterich, U. Lemmer, B. S. Richards, M. Powalla and U. W. Paetzold, *Adv. Energy Mater.*, 2019, **9**, 1–13.
180 X. Liu, Y. Xiao, Q. Zeng, J. Jiang and Y. Li, *J. Phys. Chem. Lett.*, 2019, **10**, 6382–6388.
181 B. S. Kim, T. M. Kim, M. S. Choi, H. S. Shim and J. J. Kim, *Org. Electron.*, 2015, **17**, 102–106.
182 B. Xie, Y. Zhang, Y. Li, W. Chen, X. Hu and S. Zhang, *J. Mater. Sci.: Mater. Electron.*, 2020, **31**, 6248–6254.
183 A. M. Igual-Muñoz, J. Ávila, P. P. Boix and H. J. Bolink, *Sol. RRL*, 2020, **4**, 1–5.
184 Q. Zeng, Z. Xu, C. Zheng, Y. Liu, W. Chen, T. Guo, F. Li, C. Xiang, Y. Yang, W. Cao, X. Xie, X. Yan, L. Qian and P. H. Holloway, *ACS Appl. Mater. Interfaces*, 2018, **10**, 8258–8264.
185 W. Zhang, H. Li, C. J. Firby, M. Al-Hussein and A. Y. Elezzabi, *ACS Appl. Mater. Interfaces*, 2019, **11**, 20378–20385.
186 A. Ng, Z. Ren, Q. Shen, S. H. Cheung, H. C. Gokkaya, G. Bai, J. Wang, L. Yang, S. K. So, A. B. Djurišić, W. W. F. Leung, J. Hao, W. K. Chan and C. Surya, *J. Mater. Chem. A*, 2015, **3**, 9223–9231.
187 Y. Zhao, A. M. Nardes and K. Zhu, *Appl. Phys. Lett.*, 2014, **104**, 213906.
188 P. Schulz, J. O. Tiepelt, J. A. Christians, I. Levine, E. Edri, E. M. Sanehira, G. Hodes, D. Cahen and A. Kahn, *ACS Appl. Mater. Interfaces*, 2016, **8**, 31491–31499.
189 I. S. Yang, M. R. Sohn, S. Do Sung, Y. J. Kim, Y. J. Yoo, J. Kim and W. I. Lee, *Nano Energy*, 2017, **32**, 414–421.
190 J. A. Raiford, R. A. Belisle, K. A. Bush, R. Prasanna, A. F. Palmstrom, M. D. McGehee and S. F. Bent, *Sustainable Energy Fuels*, 2019, **3**, 1517–1525.
191 S. Chu, R. Zhao, R. Liu, Y. Gao, X. Wang, C. Liu, J. Chen and H. Zhou, *Semicond. Sci. Technol.*, 2018, **33**, 115016.
192 D. Forgács, L. Gil-Escrig, D. Pérez-Del-Rey, C. Momblona, J. Werner, B. Niesen, C. Ballif, M. Sessolo and H. J. Bolink, *Adv. Energy Mater.*, 2017, **7**, 1–6.
193 Y. Zheng, J. Kong, D. Huang, W. Shi, L. Mcmillon-Brown, H. E. Katz, J. Yu and A. D. Taylor, *Nanoscale*, 2018, **10**, 11342–11348.
194 Z. Yang, C. C. Chueh, F. Zuo, J. H. Kim, P. W. Liang and A. K. Y. Jen, *Adv. Energy Mater.*, 2015, **5**, 1–6.
195 Z. Ku, Y. Rong, M. Xu, T. Liu and H. Han, *Sci. Rep.*, 2013, **3**, 3132–3137.
196 Y. Yang, K. Ri, A. Mei, L. Liu, M. Hu, T. Liu, X. Li and H. Han, *J. Mater. Chem. A*, 2015, **3**, 9103–9107.
197 B. Su, H. A. Caller-Guzman, V. Körstgens, Y. Rui, Y. Yao, N. Saxena, G. Santoro, S. V. Roth and P. Müller-Buschbaum, *ACS Appl. Mater. Interfaces*, 2017, **9**, 43724–43732.
198 K. S. Keremane, S. Prathapani, L. J. Haur, A. Bruno, A. Priyadarshi, A. V. Adhikari and S. G. Mhaisalkar, *ACS Appl. Energy Mater.*, 2021, 2–11.
199 P. Chen, Z. Wang, S. Wang, M. Lyu, M. Hao, M. Ghasemi, M. Xiao, J. H. Yun, Y. Bai and L. Wang, *Nano Energy*, 2020, **69**, 104392.
200 Q. Jiang, Y. Zhao, X. Zhang, X. Yang, Y. Chen, Z. Chu, Q. Ye, X. Li, Z. Yin and J. You, *Nat. Photonics*, 2019, **13**, 460–466.
201 Z. Ku, X. Xia, H. Shen, N. H. Tiep and H. J. Fan, *Nanoscale*, 2015, **7**, 13363–13368.
202 S. H. Lee, G. Kim, J. W. Lim, K. S. Lee and M. G. Kang, *Sol. Energy Mater. Sol. Cells*, 2018, **186**, 378–384.
203 C. Tian, A. Mei, S. Zhang, H. Tian, S. Liu, F. Qin, Y. Xiong, Y. Rong, Y. Hu, Y. Zhou, S. Xie and H. Han, *Nano Energy*, 2018, **53**, 160–167.
204 H. Chen and S. Yang, *Adv. Mater.*, 2017, **29**, 1603994.

205 T. Mahmoudi, Y. Wang and Y. B. Hahn, *Nano Energy*, 2018, **47**, 51–65.
206 E. L. Lim, C. C. Yap, M. H. H. Jumali, M. A. M. Teridi and C. H. Teh, *Nano-Micro Lett.*, 2018, **10**, 27–39.
207 Z. Liu, P. You, C. Xie, G. Tang and F. Yan, *Nano Energy*, 2016, **28**, 151–157.
208 H. Sung, N. Ahn, M. S. Jang, J. K. Lee, H. Yoon, N. G. Park and M. Choi, *Adv. Energy Mater.*, 2016, **6**, 2–7.
209 J. Yoon, H. Sung, G. Lee, W. Cho, N. Ahn, H. S. Jung and M. Choi, *Energy Environ. Sci.*, 2017, **10**, 337–345.
210 C. Zhang, S. Wang, H. Zhang, Y. Feng, W. Tian, Y. Yan, J. Bian, Y. Wang, S. Jin, S. M. Zakeeruddin, M. Grätzel and Y. Shi, *Energy Environ. Sci.*, 2019, **12**, 3585–3594.
211 Y. Yuan and J. Huang, *Acc. Chem. Res.*, 2016, **49**, 286–293.
212 M. I. Asghar, J. Zhang, H. Wang and P. D. Lund, *Renewable Sustainable Energy Rev.*, 2017, **77**, 131–146.
213 N. A. N. Ouedraogo, Y. Chen, Y. Y. Xiao, Q. Meng, C. B. Han, H. Yan and Y. Zhang, *Nano Energy*, 2020, **67**, 104249.
214 Y. Wang, Y. Zhou, T. Zhang, M. G. Ju, L. Zhang, M. Kan, Y. Li, X. C. Zeng, N. P. Padture and Y. Zhao, *Mater. Horiz.*, 2018, **5**, 868–873.
215 A. Agresti, S. Pescetelli, A. L. Palma, B. Martín-García, L. Najafi, S. Bellani, I. Moreels, M. Prato, F. Bonaccorso and A. Di Carlo, *ACS Energy Lett.*, 2019, **4**, 1862–1871.
216 J. Liu, Y. Xue, Z. Wang, Z. Q. Xu, C. Zheng, B. Weber, J. Song, Y. Wang, Y. Lu, Y. Zhang and Q. Bao, *ACS Nano*, 2016, **10**, 3536–3542.
217 J. Wu, J. Shi, Y. Li, H. Li, H. Wu and Y. Luo, *Adv. Energy Mater.*, 2019, **1901352**, 1–9.
218 X. Ren, L. Zhang, Y. Yuan and L. Ding, *J. Semicond.*, 2021, **42**, 010201.
219 H. Yu, Q. Sun, T. Zhang, X. Zhang, Y. Shen and M. Wang, *Mater. Today Energy*, 2021, **19**, 1–12.
220 E. Zheng, Z. Niu, G. A. Tosado, H. Dong, Y. Albrikan and Q. Yu, *J. Phys. Chem. C*, 2020, **124**, 18805–18815.
221 K. J. Xu, R. T. Wang, A. F. Xu, J. Y. Chen and G. Xu, *ACS Appl. Mater. Interfaces*, 2020, **12**, 48882–48889.
222 S. P. Russo and N. V Medhekar, *J. Mater. Chem. A*, 2020, **8**, 17765–17779.
223 S. Fang, W. Yao, Z. Hu, L. Huang, X. Liu, H. Zhang, J. Zhang and Y. Zhu, *J. Phys. Chem. C*, 2021, **125**, 21370–21380.
224 S. Bae, S. Kim, S. Lee, K. J. Cho, S. Park, S. Lee, Y. Kang, H. Lee and D. Kim, *J. Phys. Chem. Lett.*, 2016, **7**, 3091–3096.
225 P. Bastos, W. Song, L. Rakocevic, R. T. Eachambadi, W. Qiu, R. Gehlhaar, Y. Kuang, A. Hadipour, T. Aernouts and J. Poortmans, *ACS Appl. Mater. Interfaces*, 2021, **13**, 44294–44301.
226 F. Wan, X. Qiu, H. Chen, Y. Liu, H. Xie, J. Shi and H. Huang, *Org. Electron.*, 2018, **59**, 184–189.
227 W. Ming, D. Yang, T. Li, L. Zhang and M. Du, *Adv. Sci.*, 2018, **5**, 1700662.
228 O. A. Syzgantseva, M. Saliba, M. Gra and U. Rothlisberger, *Sci. Rep.*, 2017, **7**, 6–11.
229 S. Tang, S. Huang, G. J. Wilson and A. Ho-baillie, *Trends Chem.*, 2006, **2**, 638–653.
230 S. Bi, X. Leng, Y. Li, Z. Zheng, X. Zhang and Y. Zhang, *Adv. Mater.*, 2019, **31**, 1–8.
231 A. Agresti, S. Pescetelli, A. L. Palma, B. Mart, L. Naja, S. Bellani, I. Moreels, M. Prato, F. Bonaccorso and A. Di Carlo, *ACS Energy Lett.*, 2019, **4**, 1862–1871.
232 J. You, L. Meng, T. Bin Song, T. F. Guo, W. H. Chang, Z. Hong, H. Chen, H. Zhou, Q. Chen, Y. Liu, N. De Marco and Y. Yang, *Nat. Nanotechnol.*, 2016, **11**, 75–81.
233 W. Sun, Y. Li, S. Ye, H. Rao, W. Yan, H. Peng, Y. Li, Z. Liu, S. Wang, Z. Chen, L. Xiao, Z. Bian and C. Huang, *Nanoscale*, 2016, **8**, 10806–10813.
234 S. Ye, W. Sun, Y. Li, W. Yan, H. Peng, Z. Bian, Z. Liu and C. Huang, *Nano Lett.*, 2015, **15**, 3723–3728.
235 Microquanta demonstrates high stability beyond IEC standards, http://www.microquanta.com/en/newsinfo/112E5B4ABC180F9D/.
236 M. V. Khenkin, E. A. Katz, A. Abate, G. Bardizza, J. J. Berry, C. Brabec, F. Brunetti, V. Bulović, Q. Burlingame, A. Di Carlo, R. Cheacharoen, Y. B. Cheng, A. Colsmann, S. Cros, K. Domanski, M. Dusza, C. J. Fell, S. R. Forrest, Y. Galagan, D. Di Girolamo, M. Grätzel, A. Hagfeldt, E. von Hauff, H. Hoppe, J. Kettle, H. Köbler, M. S. Leite, S. (Frank) Liu, Y. L. Loo, J. M. Luther, C. Q. Ma, M. Madsen, M. Manceau, M. Matheron, M. McGehee, R. Meitzner, M. K. Nazeeruddin, A. F. Nogueira, Ç. Odabaşı, A. Osherov, N. G. Park, M. O. Reese, F. De Rossi, M. Saliba, U. S. Schubert, H. J. Snaith, S. D. Stranks, W. Tress, P. A. Troshin, V. Turkovic, S. Veenstra, I. Visoly-Fisher, A. Walsh, T. Watson, H. Xie, R. Yıldırım, S. M. Zakeeruddin, K. Zhu and M. Lira-Cantu, *Nat. Energy*, 2020, **5**, 35–49.
237 Z. Yang, S. Zhang, L. Li and W. Chen, *J. Mater.*, 2017, **3**, 231–244.
238 N. Li, X. Niu, Q. Chen and H. Zhou, *Chem. Soc. Rev.*, 2020, **49**, 8235–8286.
239 Q. Wali, F. J. Iftikhar, M. E. Khan, A. Ullah, Y. Iqbal and R. Jose, *Org. Electron.*, 2020, **78**, 105590.
240 S. Zhang, Z. Liu, W. Zhang, Z. Jiang, W. Chen, R. Chen, Y. Huang, Z. Yang, Y. Zhang, L. Han and W. Chen, *Adv. Energy Mater.*, 2020, **10**, 1–49.
241 M. K. Rao, D. N. Sangeetha, M. Selvakumar, Y. N. Sudhakar and M. G. Mahesha, *Sol. Energy*, 2021, **218**, 469–491.
242 U. Krishnan, *J. Photonics Energy*, 2019, **9**, 1.
243 A. Priyadarshi, L. J. Haur, P. Murray, D. Fu, S. Kulkarni, G. Xing, T. C. Sum, N. Mathews and S. G. Mhaisalkar, *Energy Environ. Sci.*, 2016, **9**, 3687–3692.
244 A. Mei, X. Li, L. Liu, Z. Ku, T. Liu, Y. Rong, M. Xu, M. Hu, J. Chen, Y. Yang, M. Grätzel and H. Han, *Science*, 2014, **345**, 295–298.
245 H. Tan, E. Moulin, T. F. Si, J.-W. Schüttauf, M. Stuckelberger, O. Isabella, F. J. Haug, C. Ballif, M. Zeman and A. H. M. Smets, *Prog. Photovolt. Res. Appl.*, 2015, **23**, 949–963.
246 T. Matsui, K. Maejima, A. Bidiville, H. Sai, T. Koida, T. Suezaki, M. Matsumoto, K. Saito, I. Yoshida and M. Kondo, *Jpn. J. Appl. Phys.*, 2015, **54**, 10–14.
247 J. S. Cashmore, M. Apolloni, A. Braga, O. Caglar, V. Cervetto, Y. Fenner, S. Goldbach-Aschemann, C. Goury, J. E. Hötzel, T. Iwahashi, J. Kalas, M. Kitamura,

M. Klindworth, M. Kupich, G. F. Leu, J. Lin, M. H. Lindic, P. A. Losio, T. Mates, D. Matsunaga, B. Mereu, X. V. Nguyen, I. Psimoulis, S. Ristau, T. Roschek, A. Salabas, E. L. Salabas and I. Sinicco, *Sol. Energy Mater. Sol. Cells*, 2016, **144**, 84–95.

248 S. Kim, J. W. Chung, H. Lee, J. Park, Y. Heo and H. M. Lee, *Sol. Energy Mater. Sol. Cells*, 2013, **119**, 26–35.

249 B. Liu, L. Bai, Z. Chen, X. Zhang, D. Zhang, J. Ni, Q. Huang, C. Wei, J. Sun, X. Chen, H. Ren, G. Hou, G. Wang and Y. Zhao, *Prog. Photovolt. Res. Appl.*, 2015, **23**, 1313–1322.

250 K. Söderström, G. Bugnon, R. Biron, C. Pahud, F. Meillaud, F. J. Haug and C. Ballif, *J. Appl. Phys.*, 2012, **112**, 114503.

251 B. Yan, G. Yue, L. Sivec, J. Yang, S. Guha and C. S. Jiang, *Appl. Phys. Lett.*, 2011, **99**, 113512.

252 H. Sai, T. Matsui and K. Matsubara, *Appl. Phys. Lett.*, 2016, **109**, 1–6.

253 F. J. Haug and C. Ballif, *Energy Environ. Sci.*, 2015, **8**, 824–837.

254 O. Isabella, A. H. M. Smets and M. Zeman, *Sol. Energy Mater. Sol. Cells*, 2014, **129**, 82–89.

255 F. T. Si, D. Y. Kim, R. Santbergen, H. Tan, R. A. C. M. M. Van Swaaij, A. H. M. Smets, O. Isabella and M. Zeman, *Appl. Phys. Lett.*, 2014, **105**, 063902.

256 S. Kirner, S. Neubert, C. Schultz, O. Gabriel, B. Stannowski, B. Rech and R. Schlatmann, *Jpn. J. Appl. Phys.*, 2015, **54**, 03.

257 M. Konagai, H. Noge and R. Ishikawa, *Prog. Photovolt. Res. Appl.*, 2020, 1–7.

258 T. Takamoto, H. Washio and H. Huso, *Proc. 40 th IEEE PVSC*, 2014, pp. 5–9.

259 N. Jain, K. L. Schulte, J. F. Geisz, D. J. Friedman, R. M. France, E. E. Perl, A. G. Norman, H. L. Guthrey and M. A. Steiner, *Appl. Phys. Lett.*, 2018, **112**, 053905.

260 F. Dimroth, T. N. D. Tibbits, M. Niemeyer, F. Predan, P. Beutel, C. Karcher, E. Oliva, G. Siefer, D. Lackner, P. Fus-Kailuweit, A. W. Bett, R. Krause, C. Drazek, E. Guiot, J. Wasselin, A. Tauzin and T. Signamarcheix, *IEEE J. Photovoltaics*, 2016, **6**, 343–349.

261 J. F. Geisz, M. A. Steiner, N. Jain, K. L. Schulte, R. M. France, W. E. McMahon, E. E. Perl and D. J. Friedman, *IEEE J. Photovoltaics*, 2018, **8**, 626–632.

262 K. Sasaki, T. Agui, K. Nakaido, N. Takahashi, R. Onitsuka and T. Takamoto, *AIP Conf. Proc.*, 2013, **1556**, 22–25.

263 P. T. Chiu, D. C. Law, R. L. Woo, S. B. Singer, D. Bhusari, W. D. Hong, A. Zakaria, J. Boisvert, S. Mesropian, R. R. King and N. H. Karam, *2014 IEEE 40th Photovolt. Spec. Conf. PVSC 2014*, 2014, pp. 11–13.

264 MicroLink Device Inc, *MicroLink AFWERX Phase I Projects*, 2021.

265 NREL, *News Release: NREL Demonstrates 45.7% Efficiency for Concentrator Solar Cell*, 2014.

266 SHARP, *Sharp Develops Concentrator Solar Cell with World's Highest Conversion Efficiency of 43.5%*, 2012.

267 Z. Yu, M. Leilaeioun and Z. Holman, *Nat. Energy*, 2016, **1**, 16137.

268 E. L. Warren, W. E. Mcmahon, M. Rienäcker, K. T. Vansant, R. C. Whitehead, R. Peibst and A. C. Tamboli, *ACS Energy Lett.*, 2020, **5**, 1233–1242.

269 M. Rienäcker, E. L. Warren, M. Schnabel, H. Schulte-Huxel, R. Niepelt, R. Brendel, P. Stradins, A. C. Tamboli and R. Peibst, *Prog. Photovolt. Res. Appl.*, 2019, **27**, 410–423.

270 J. P. Connolly, K. Ahanobge, J.-P. Kleider, J. Alvarez, H. Kanda, M. Nazeeruddin, V. Mihailetchi, P. Baranek, M. Vogt, R. Santbergen, J. P. Kleider, M. K. Nazeeruddin, V. Mihailetchi, P. Baranek and O. Isabella, *37th European Photovoltaic Solar Energy Conference and Exhibition (EU PVSEC)*, 2020.

271 B. Ehrler, E. Alarcón-Lladó, S. W. Tabernig, T. Veeken, E. C. Garnett and A. Polman, *ACS Energy Lett.*, 2020, **5**, 3029–3033.

272 T. C. J. Yang, P. Fiala, Q. Jeangros and C. Ballif, *Joule*, 2018, **2**, 1421–1436.

273 R. Comin, G. Walters, E. S. Thibau, O. Voznyy, Z. H. Lu and E. H. Sargent, *J. Mater. Chem. C*, 2015, **3**, 8839–8843.

274 N. Yaghoobi Nia, D. Saranin, A. L. Palma and A. Di Carlo, *Sol. Cells Light Manag. Mater. Strateg. Sustain.*, 2019, pp. 163–228.

275 H. Shen, T. Duong, J. Peng, D. Jacobs, N. Wu, J. Gong, Y. Wu, S. K. Karuturi, X. Fu, K. Weber, X. Xiao, T. P. White and K. Catchpole, *Energy Environ. Sci.*, 2018, **11**, 394–406.

276 T. J. Jacobsson, A. Hultqvist, S. Svanström, L. Riekehr, U. B. Cappel, E. Unger, H. Rensmo, E. M. J. Johansson, M. Edoff and G. Boschloo, *Sol. Energy*, 2020, **207**, 270–288.

277 Breakthrough: thin-film solar cells generate as much energy as traditional solar cells for the first time, https://www.imec-int.com/en/articles/breakthrough-thin-film-solar-cells-generate-as-much-energy-as-traditional-solar-cells-for-the-first-time.

278 Y. Cheng and L. Ding, *SusMat*, 2021, **1**, 324–344.

279 S. Chauhan and R. Singh, *Preprints*, 2021, 1–25.

280 N. N. Lal, Y. Dkhissi, W. Li, Q. Hou, Y. B. Cheng and U. Bach, *Adv. Energy Mater.*, 2017, **7**, 1–18.

281 L. L. Yan, C. Han, B. Shi, Y. Zhao and X. D. Zhang, *Mater. Today Nano*, 2019, **7**, 100045.

282 Q. Wali, N. K. Elumalai, Y. Iqbal, A. Uddin and R. Jose, *Renewable Sustainable Energy Rev.*, 2018, **84**, 89–110.

283 J. Werner, L. Barraud, A. Walter, M. Bräuninger, F. Sahli, D. Sacchetto, N. Tétreault, B. Paviet-Salomon, S. J. Moon, C. Allebé, M. Despeisse, S. Nicolay, S. De Wolf, B. Niesen and C. Ballif, *ACS Energy Lett.*, 2016, **1**, 474–480.

284 Z. Wang, X. Zhu, S. Zuo, M. Chen, C. Zhang, C. Wang, X. Ren, Z. Yang, Z. Liu, X. Xu, Q. Chang, S. Yang, F. Meng, Z. Liu, N. Yuan, J. Ding, S. Liu and D. Yang, *Adv. Funct. Mater.*, 2020, **30**, 1–8.

285 H. Shen, S. T. Omelchenko, D. A. Jacobs, S. Yalamanchili, Y. Wan, D. Yan, P. Phang, T. Duong, Y. Wu, Y. Yin, C. Samundsett, J. Peng, N. Wu, T. P. White, G. G. Andersson, N. S. Lewis and K. R. Catchpole, *Sci. Adv.*, 2018, 4, DOI: 10.1126/sciadv.aau9711.

286 Y. Hou, E. Aydin, M. De Bastiani, C. Xiao, F. H. Isikgor, D. J. Xue, B. Chen, H. Chen, B. Bahrami, A. H. Chowdhury, A. Johnston, S. W. Baek, Z. Huang, M. Wei, Y. Dong, J. Troughton, R. Jalmood, A. J. Mirabelli, T. G. Allen, E. Van Kerschaver,

M. I. Saidaminov, D. Baran, Q. Qiao, K. Zhu, S. De Wolf and E. H. Sargent, *Science*, 2020, **367**, 1135–1140.

287 J. K. Hwang, S. W. Lee, W. Lee, S. Bae, K. Cho, S. Kim, S. Lee, J. Y. Hyun, Y. Kang, H. S. Lee and D. Kim, *Thin Solid Films*, 2020, **693**, 137694.

288 A. S. Subbiah, F. H. Isikgor, C. T. Howells, M. De Bastiani, J. Liu, E. Aydin, F. Furlan, T. G. Allen, F. Xu, S. Zhumagali, S. Hoogland, E. H. Sargent, I. McCulloch and S. De Wolf, *ACS Energy Lett.*, 2020, **5**, 3034–3040.

289 K. A. Bush, A. F. Palmstrom, Z. J. Yu, M. Boccard, R. Cheacharoen, J. P. Mailoa, D. P. McMeekin, R. L. Z. Hoye, C. D. Bailie, T. Leijtens, I. M. Peters, M. C. Minichetti, N. Rolston, R. Prasanna, S. Sofia, D. Harwood, W. Ma, F. Moghadam, H. J. Snaith, T. Buonassisi, Z. C. Holman, S. F. Bent and M. D. McGehee, *Nat. Energy*, 2017, **2**, 1–7.

290 J. Werner, C. H. Weng, A. Walter, L. Fesquet, J. P. Seif, S. De Wolf, B. Niesen and C. Ballif, *J. Phys. Chem. Lett.*, 2016, **7**, 161–166.

291 J. Zheng, C. F. J. Lau, H. Mehrvarz, F. J. Ma, Y. Jiang, X. Deng, A. Soeriyadi, J. Kim, M. Zhang, L. Hu, X. Cui, D. S. Lee, J. Bing, Y. Cho, C. Chen, M. A. Green, S. Huang and A. W. Y. Ho-Baillie, *Energy Environ. Sci.*, 2018, **11**, 2432–2443.

292 Y. Wu, D. Yan, J. Peng, T. Duong, Y. Wan, S. P. Phang, H. Shen, N. Wu, C. Barugkin, X. Fu, S. Surve, D. Grant, D. Walter, T. P. White, K. R. Catchpole and K. J. Weber, *Energy Environ. Sci.*, 2017, **10**, 2472–2479.

293 E. Köhnen, M. Jošt, A. B. Morales-Vilches, P. Tockhorn, A. Al-Ashouri, B. Macco, L. Kegelmann, L. Korte, B. Rech, R. Schlatmann, B. Stannowski and S. Albrecht, *Sustainable Energy Fuels*, 2019, **3**, 1995–2005.

294 M. De Bastiani, A. S. Subbiah, E. Aydin, F. H. Isikgor, T. G. Allen and S. De Wolf, *Mater. Horiz.*, 2020, **7**, 2791–2809.

295 B. A. Kamino, B. Paviet-Salomon, S. J. Moon, N. Badel, J. Levrat, G. Christmann, A. Walter, A. Faes, L. Ding, J. J. Diaz Leon, A. Paracchino, M. Despeisse, C. Ballif and S. Nicolay, *ACS Appl. Energy Mater.*, 2019, **2**, 3815–3821.

296 F. Sahli, B. A. Kamino, J. Werner, M. Bräuninger, B. Paviet-Salomon, L. Barraud, R. Monnard, J. P. Seif, A. Tomasi, Q. Jeangros, A. Hessler-Wyser, S. De Wolf, M. Despeisse, S. Nicolay, B. Niesen and C. Ballif, *Adv. Energy Mater.*, 2018, **8**, 1–8.

297 M. Singh, *Nanophotonics*, 2021, accepted for publication.

298 D. A. Jacobs, M. Langenhorst, F. Sahli, B. S. Richards, T. P. White, C. Ballif, K. R. Catchpole and U. W. Paetzold, *J. Phys. Chem. Lett.*, 2019, **10**, 3159–3170.

299 F. Hou, C. Han, O. Isabella, L. Yan, B. Shi, J. Chen, S. An, Z. Zhou, W. Huang, H. Ren, Q. Huang, G. Hou, X. Chen, Y. Li, Y. Ding, G. Wang, C. Wei, D. Zhang, M. Zeman, Y. Zhao and X. Zhang, *Nano Energy*, 2019, **56**, 234–240.

300 K. A. Bush, S. Manzoor, K. Frohna, Z. J. Yu, J. A. Raiford, A. F. Palmstrom, H. P. Wang, R. Prasanna, S. F. Bent, Z. C. Holman and M. D. McGehee, *ACS Energy Lett.*, 2018, **3**, 2173–2180.

301 M. Jošt, E. Köhnen, A. B. Morales-Vilches, B. Lipovšek, K. Jäger, B. Macco, A. Al-Ashouri, J. Krč, L. Korte, B. Rech, R. Schlatmann, M. Topič, B. Stannowski and S. Albrecht, *Energy Environ. Sci.*, 2018, **11**, 3511–3523.

302 L. Mazzarella, Y. H. Lin, S. Kirner, A. B. Morales-Vilches, L. Korte, S. Albrecht, E. Crossland, B. Stannowski, C. Case, H. J. Snaith and R. Schlatmann, *Adv. Energy Mater.*, 2019, **9**, 1–9.

303 J. Zheng, H. Mehrvarz, C. Liao, J. Bing, X. Cui, Y. Li, V. R. Gonçales, C. F. J. Lau, D. S. Lee, Y. Li, M. Zhang, J. Kim, Y. Cho, L. G. Caro, S. Tang, C. Chen, S. Huang and A. W. Y. Ho-Baillie, *ACS Energy Lett.*, 2019, **4**, 2623–2631.

304 J. P. Mailoa, C. D. Bailie, E. C. Johlin, E. T. Hoke, A. J. Akey, W. H. Nguyen, M. D. McGehee and T. Buonassisi, *Appl. Phys. Lett.*, 2015, **106**, 121105.

305 J. Werner, A. Walter, E. Rucavado, S. J. Moon, D. Sacchetto, M. Rienaecker, R. Peibst, R. Brendel, X. Niquille, S. De Wolf, P. Löper, M. Morales-Masis, S. Nicolay, B. Niesen and C. Ballif, *Appl. Phys. Lett.*, 2016, **109**, 233902.

306 G. Nogay, F. Sahli, J. Werner, R. Monnard, M. Boccard, M. Despeisse, F. J. Haug, Q. Jeangros, A. Ingenito and C. Ballif, *ACS Energy Lett.*, 2019, **4**, 844–845.

307 A. Al-Ashouri, E. Köhnen, B. Li, A. Magomedov, H. Hempel, P. Caprioglio, J. A. Márquez, A. B. M. Vilches, E. Kasparavicius, J. A. Smith, N. Phung, D. Menzel, M. Grischek, L. Kegelmann, D. Skroblin, C. Gollwitzer, T. Malinauskas, M. Jošt, G. Matič, B. Rech, R. Schlatmann, M. Topič, L. Korte, A. Abate, B. Stannowski, D. Neher, M. Stolterfoht, T. Unold, V. Getautis and S. Albrecht, *Science*, 2020, **370**, 1300–1309.

308 D. Kim, H. J. Jung, I. J. Park, B. W. Larson, S. P. Dunfield, C. Xiao, J. Kim, J. Tong, P. Boonmongkolras, S. G. Ji, F. Zhang, S. R. Pae, M. Kim, S. B. Kang, V. Dravid, J. J. Berry, J. Y. Kim, K. Zhu, D. H. Kim and B. Shin, *Science*, 2020, **368**, 155–160.

309 J. Xu, C. C. Boyd, Z. J. Yu, A. F. Palmstrom, D. J. Witter, B. W. Larson, R. M. France, J. Werner, S. P. Harvey, E. J. Wolf, W. Weigand, S. Manzoor, M. F. A. M. Van Hest, J. J. Berry, J. M. Luther, Z. C. Holman and M. D. McGehee, *Science*, 2020, **367**, 1097–1104.

310 E. Lamanna, F. Matteocci, E. Calabrò, L. Serenelli, E. Salza, L. Martini, F. Menchini, M. Izzi, A. Agresti, S. Pescetelli, S. Bellani, A. E. Del Río Castillo, F. Bonaccorso, M. Tucci and A. Di Carlo, *Joule*, 2020, **4**, 865–881.

311 A. Al-Ashouri, A. Magomedov, M. Roß, M. Jošt, M. Talaikis, G. Chistiakova, T. Bertram, J. A. Márquez, E. Köhnen, E. Kasparavičius, S. Levcenco, L. Gil-Escrig, C. J. Hages, R. Schlatmann, B. Rech, T. Malinauskas, T. Unold, C. A. Kaufmann, L. Korte, G. Niaura, V. Getautis and S. Albrecht, *Energy Environ. Sci.*, 2019, **12**, 3356–3369.

312 J. Zheng, H. Mehrvarz, F. J. Ma, C. F. J. Lau, M. A. Green, S. Huang and A. W. Y. Ho-Baillie, *ACS Energy Lett.*, 2018, **3**, 2299–2300.

313 N. G. Park, M. Grätzel, T. Miyasaka, K. Zhu and K. Emery, *Nat. Energy*, 2016, **1**, 16152.

314 Z. Song, C. L. McElvany, A. B. Phillips, I. Celik, P. W. Krantz, S. C. Watthage, G. K. Liyanage, D. Apul and M. J. Heben, *Energy Environ. Sci.*, 2017, **10**, 1297–1305.
315 NREL, https://www.nrel.gov/pv/news.html.
316 K. A. W. Horowitz, R. Fu and M. Woodhouse, *Sol. Energy Mater. Sol. Cells*, 2016, **154**, 1–10.
317 N. L. Chang, A. W. Y. Ho-Baillie, D. Vak, M. Gao, M. A. Green and R. J. Egan, *Sol. Energy Mater. Sol. Cells*, 2018, **174**, 314–324.
318 M. Cai, Y. Wu, H. Chen, X. Yang, Y. Qiang and L. Han, *Adv. Sci.*, 2017, **4**, 1600269.
319 N. L. Chang, A. W. Yi Ho-Baillie, P. A. Basore, T. L. Young, R. Evans and R. J. Egan, *Prog. Photovolt. Res. Appl.*, 2017, **25**, 390–405.
320 N. L. Chang, J. Zheng, Y. Wu, H. Shen, F. Qi, K. Catchpole, A. Ho-Baillie and R. J. Egan, *Prog. Photovolt. Res. Appl.*, 2021, **29**, 401–413.
321 C. Messmer, B. S. Goraya, S. Nold, P. S. C. Schulze, V. Sittinger, J. Schön, J. C. Goldschmidt, M. Bivour, S. W. Glunz and M. Hermle, *Prog. Photovolt. Res. Appl.*, 2021, **29**, 744–759.
322 F. Ise, ISE, Photovoltaics Report, 2020.
323 Z. Li, Y. Zhao, X. Wang, Y. Sun, Z. Zhao, Y. Li, H. Zhou and Q. Chen, *Joule*, 2018, **2**, 1559–1572.
324 L. A. Zafoschnig, S. Nold and J. C. Goldschmidt, *IEEE J. Photovoltaics*, 2020, **10**, 1632–1641.
325 S. E. Sofia, H. Wang, A. Bruno, J. L. Cruz-Campa, T. Buonassisi and I. M. Peters, *Sustainable Energy Fuels*, 2020, **4**, 852–862.
326 S. E. Sofia, H. Wang, A. Bruno, T. Buonassisi and I. M. Peters, *Conf. Rec. IEEE Photovolt. Spec. Conf.*, 2019, pp. 572–576.
327 T. P. Gujar and M. Thelakkat, *Energy Technol.*, 2016, **4**, 449–457.
328 M. R. Leyden, M. V. Lee, S. R. Raga and Y. Qi, *J. Mater. Chem. A*, 2015, **3**, 16097–16103.
329 J. Borchert, I. Levchuk, L. C. Snoek, M. U. Rothmann, R. Haver, H. J. Snaith, C. J. Brabec, L. M. Herz and M. B. Johnston, *ACS Appl. Mater. Interfaces*, 2019, **11**, 28851–28857.
330 H. Zhang, J. Cheng, F. Lin, H. He, J. Mao, K. S. Wong, A. K. Y. Jen and W. C. H. Choy, *ACS Nano*, 2016, **10**, 1503–1511.
331 S. R. Pae, S. Byun, J. Kim, M. Kim, I. Gereige and B. Shin, *ACS Appl. Mater. Interfaces*, 2018, **10**, 534–540.
332 Ç. Odabaşı and R. Yıldırım, *Energy Technol.*, 2020, **1901449**, 1–12.
333 J. Gong, S. B. Darling and F. You, *Energy Environ. Sci.*, 2015, **8**, 1953–1968.
334 A. Urbina, *J. Phys.: Energy*, 2020, **2**, 022001.
335 T. Ibn-Mohammed, S. C. L. Koh, I. M. Reaney, A. Acquaye, G. Schileo, K. B. Mustapha and R. Greenough, *Renewable Sustainable Energy Rev.*, 2017, **80**, 1321–1344.
336 I. Celik, Z. Song, A. J. Cimaroli, Y. Yan, M. J. Heben and D. Apul, *Sol. Energy Mater. Sol. Cells*, 2016, **156**, 157–169.
337 M. Green, K. Emery, Y. Hishikawa, W. Warta, E. Dunlop, D. Barkhouse, O. Gunawan, T. Gokmen, T. Todorov and D. Mitzi, *IEEE Trans. Fuzzy Syst.*, 2012, **20**, 1114–1129.
338 J. Qian, M. Ernst, N. Wu and A. Blakers, *Sustainable Energy Fuels*, 2019, **3**, 1439–1447.
339 R. Itten and M. Stucki, *Energies*, 2017, **10**, 841.
340 X. Tian, S. D. Stranks and F. You, *Sci. Adv.*, 2020, **6**, 55–65.
341 D. A. R. Barkhouse, O. Gunawan, T. Gokmen, T. K. Todorov and D. B. Mitzi, *Prog. Photovolt. Res. Appl.*, 2015, **20**, 6–11.
342 E. Leccisi and V. Fthenakis, *Prog. Energy*, 2020, **2**, 032002.
343 Energy Materials Corporation (n.d.), https://www.perovskite-info.com/energy-materials-corp-emc.
344 Saule Technologies (n.d.), https://www.perovskite-info.com/inkjet-printed-flexible-perovskite-leds-could-open-door-new-applications.
345 M. A. Green, Y. Hishikawa, E. D. Dunlop, D. H. Levi, J. Hohl-Ebinger and A. W. Y. Ho-Baillie, *Prog. Photovolt. Res. Appl.*, 2018, **26**, 427–436.
346 Oxford Photovoltaics (n.d.), https://www.oxfordpv.com/news/oxford-pv-hits-new-world-record-solar-cell.
347 Greatcell Solar. (n.d.), http://www.osadirect.com/news/article/2154/greatcell-solar-has-receives-eu-horizon-2020-project-award-of-500000/.
348 L. Cai, L. Liang, J. Wu, B. Ding, L. Gao and B. Fan, *J. Semicond.*, 2017, **38**, 014006.
349 Solaronix. (n.d.), https://www.solaronix.com/news/solaronix-achieves-major-breakthrough-toward-perovskite-solar-cell-industrialization/.
350 M. A. Green, E. D. Dunlop, J. Hohl-Ebinger, M. Yoshita, N. Kopidakis and A. W. Y. Ho-Baillie, *Prog. Photovolt. Res. Appl.*, 2020, **28**, 3–15.
351 *Swift Solar Looks to Reinvigorate and Push the Perovskite Market Forward*, 2020, https://pv-magazine-usa.com/2020/10/08/swift-solar-looks-to-reinvigorate-and-push-the-perovskite-market-forward/.
352 Oxford PV, 2020, https://www.oxfordpv.com/.

